

BDNF is a prognostic biomarker involved in the immune infiltration of lung adenocarcinoma and associated with programmed cell death

JIANGNAN XIA¹, WEI ZHUO¹, LILAN DENG¹, SHENG YIN¹, SHUANGQIN TANG¹, LIJUAN YI¹,
CHUANPING FENG¹, XIANGYUN ZHONG¹, ZHIJUN HE¹, BIQIANG SUN^{1*} and CHI ZHANG^{2*}

¹College of Pharmacy, Hunan Traditional Chinese Medical College, Zhuzhou, Hunan 412012, P.R. China;

²Department of Oncology, Dongfang Hospital, Beijing University of Chinese Medicine, Beijing 100078, P.R. China

Received September 25, 2024; Accepted January 15, 2025

DOI: 10.3892/ol.2025.14937

Abstract. It is well established that genes associated with cell death can serve as prognostic markers for patients with cancer. Programmed cell death (PCD) is known to play a role in cancer cell apoptosis and antitumor immunity. With the continuous discovery of new forms of PCD, the roles of PCD in lung adenocarcinoma (LUAD) require ongoing evaluation. In the present study, mRNA expression data and clinical information associated with 15 forms of PCD were extracted from publicly available databases and systematically analyzed. Utilizing these data, a robust risk prediction model was established that incorporates six PCD-related genes (PRGs). Datasets from the Gene Expression Omnibus database were employed to validate the six genes exhibiting risk-associated characteristics. The PRG-based model reliably predicted the prognosis of patients with LUAD, with the high-risk group showing a poor prognosis,

reduced levels of immune infiltration molecules and diminished expression of human leukocyte antigens. Additionally, the relationships among PRGs, somatic mutations, tumor stemness index and immune infiltration were assessed. Based on these risk characteristics, a nomogram was constructed, patient stratification was performed, small-molecule drug candidates were predicted, and somatic mutations and chemotherapy responses were analyzed. Furthermore, reverse transcription-quantitative PCR was used to assess the expression of PDGs *in vitro*, and the critical role of brain-derived neurotrophic factor in LUAD development was identified through Mendelian randomization, gene knockdown, wound healing, western blot and colony formation assays. These findings offer new insights into the development of targeted therapies for LUAD, particularly in patients with high BDNF expression.

Correspondence to: Dr Chi Zhang, Department of Oncology, Dongfang Hospital, Beijing University of Chinese Medicine, 6 Fangxingyuan, Fengtai, Beijing 100078, P.R. China
E-mail: ydksbs@163.com

Dr Biqiang Sun, College of Pharmacy, Hunan Traditional Chinese Medical College, 136 Lusong Road, Lusong, Zhuzhou, Hunan 412012, P.R. China
E-mail: qbs912@126.com

*Contributed equally

Abbreviations: LUAD, lung adenocarcinoma; PCD, programmed cell death; BDNF, brain-derived neurotrophic factor; ADRB2, adrenergic receptor b2; ANGPTL4, angiopoietin-like protein 4; CTLA4, cytotoxic T lymphocyte-associated protein 4; GPER1, G protein-coupled estrogen receptor 1; LAMB3, laminin b3; MAP6, microtubule associated protein 6; PD-1, programmed cell death protein 1; PD-L1, programmed cell death ligand 1; ROC, receiver operating characteristic

Key words: lung cancer, prognostic model, bioinformatics, immune infiltration, programmed cell death

Introduction

Lung cancer, a malignancy arising from the bronchial mucosal epithelium and mucous glands, was estimated to account for ~2.2 million new cases of cancer and 1.8 million deaths worldwide in 2020 (1). Lung cancer is broadly classified into small cell lung cancer (SCLC), which comprises ~15% of cases, and non-SCLC (NSCLC), which comprises ~75% of cases (2). NSCLC can be further histologically subdivided into lung adenocarcinoma (LUAD), large cell carcinoma and lung squamous cell carcinoma (3). LUAD accounts for ~50% of all lung cancer diagnoses, with the majority of patients receiving their diagnosis at either intermediate or advanced stages (4). Therapy for patients with LUAD typically involves a combination of chemotherapy, immunotherapy, targeted therapy, radiation and surgery; however, the 5-year survival rate for LUAD patients remains at ~15% (5). **In addition, these treatments are frequently associated with marked therapy-related toxicity and surgical risks, resulting in poor clinical outcomes for those with advanced LUAD. Therefore, the development of strategies to identify patients who may benefit from more aggressive therapeutic interventions is urgently required. Consequently, the identification of novel diagnostic biomarkers for prognostication and therapeutic response in patients with LUAD is critically important.**

Cell death is a crucial physiological process in all living organisms, as it plays a key role in embryonic development, the upkeep of organ structure and function, tumor formation and immune responses (6). Programmed cell death (PCD) is an important mode of cell death, characterized by various complex mechanisms that interact with each other. PCD comprises a broad spectrum of distinct cellular death mechanisms, including necroptosis, apoptosis, pyroptosis, ferroptosis, lysosome-dependent cell death, entotic cell death, parthanatos, oxoapoptosis, autophagy, alkaliptosis, disulfidptosis and cuproptosis, (7). PCD is essential for modulating the immunosuppressive environment within tumors, influencing patient prognosis and determining treatment responsiveness (8). In recent years, numerous researchers have demonstrated that apoptotic inducers prolong the survival of patients with advanced, metastatic or recurrent tumors, by reducing recurrence and metastasis (9). Autophagy is a mechanism with both detrimental and beneficial effects, as it confers chemoresistance and promotes cell survival, while in some cases, it also enhances sensitivity to chemotherapy and leads to cell death. Clinical studies have explored the use of small molecule modulators and natural compounds targeting autophagy to modify cancer cell responses to chemotherapy, achieving varying degrees of success (10). Cuproptosis (11), ferroptosis (12), PANoptosis (13) and disulfidptosis (14) have emerged as important areas of research, closely associated with the tumor immune microenvironment. In addition, researchers have constructed predictive models based on PCD-related genes (PRGs), which have achieved success in malignant tumors such as lung cancer (15), hepatocellular carcinoma (16) and gastric cancer (17). Thus, the examination of genes associated with PCD may assist clinicians in the prediction of survival outcomes and the development of personalized treatment strategies for patients with cancer. Nonetheless, numerous studies focus on a single mechanism of PCD, which introduces limitations. It remains necessary to enhance the effectiveness of PCD-based predictive models. With the discovery of several new types of PCD, including PANoptosis, cuproptosis and disulfidptosis, it is crucial to update the molecular functions, prognostic value and expression patterns of PRGs in LUAD.

Neurotrophic factors (NTs) are crucial in the development, survival and health of the central and peripheral nervous systems. The mammalian NT family includes nerve growth factor, brain-derived neurotrophic factor (BDNF), NT-3 and NT-4/5 (18). Previous studies have shown that both squamous cell carcinoma and LUAD exhibit elevated expression levels of BDNF at the protein and mRNA levels (18,19). BDNF activity is mediated by its high-affinity tyrosine kinase receptor, known as tropomyosin receptor kinase B (TrkB). This activates various downstream signaling pathways, including the PI3K/AKT, RAS/ERK, Jak/STAT, phospholipase C/protein kinase C and AMP-activated protein kinase/acetyl CoA carboxylase pathways, thereby promoting lung cancer growth, metastasis and chemoresistance (20,21). Clinical analysis has also confirmed that high BDNF expression is associated with poor prognosis in patients with lung cancer (22). Although the role of BDNF in the promotion of lung cancer growth is well established, preliminary investigations suggest that BDNF may also be involved in the regulation of PCD, thereby influencing the survival and invasiveness of lung cancer cells.

The aim of the present study was to identify genes associated with 15 distinct PCD types that are differentially

expressed between LUAD and normal samples, and to develop a predictive tool to investigate the potential role of PRGs in LUAD. With the increased application of personalized medicine and immunotherapy in clinical practice, immune infiltration has increasingly become a key prognostic marker for various cancer types (23). Therefore, the present study also aimed to predict biomarkers of the tumor microenvironment (TME), characterize the immune landscape, assess drug sensitivities and analyze somatic mutations in patients stratified by risk, as well as to propose novel clinical therapies for those with LUAD. Furthermore, through bioinformatics, Mendelian randomization (MR) and cellular experiments, the study investigated the critical role of BDNF in the regulation of PCD in lung cancer. The findings of the study may provide valuable insights that could contribute to personalized treatment strategies for patients with lung cancer.

Materials and methods

Acquisition of RNA-sequencing transcriptomic data. RNA-sequencing transcriptomic information and associated clinical data for 15 patterns of PCD were obtained from The Cancer Genome Atlas (TCGA; <https://portal.gdc.cancer.gov/>; using lung adenocarcinoma as a key word). This dataset comprised 412 LUAD cases with 43 adjacent normal tissue samples. Clinical variables for the patients were collected, included sex, age, tumor stage and Tumor-Node-Metastasis (TNM) classification. In total, 1,670 PRGs were acquired via screening the GeneCards database (<https://www.genecards.org/>) and reviewing relevant literature. Expression data for these 1,670 PRGs were extracted from TCGA LUAD cohort for further analysis. To validate the findings obtained from TCGA data, four datasets from the Gene Expression Omnibus (GEO; <http://www.ncbi.nlm.nih.gov/geo>) were employed: GSE8894 (24), GSE31201 (25), GSE30219 (26) and GSE42127 (27). A comprehensive list of the analyzed genes is presented in Table S1.

Identification of PRGs in LUAD. Wilcoxon test in R (version R 4.1.2; www.r-project.org) was used to determine differentially expressed PRGs between adjacent normal and LUAD tissues. The criteria for significance included a false discovery rate (FDR) <0.05 and an absolute \log_2 -fold change >1. The vioplot R package (<https://rdocumentation.org/packages/vioplot/versions/0.4.0>) was utilized to produce heatmaps and volcano plots, which visually depict the differential expression of PRGs in LUAD compared with that in adjacent normal tissue.

Weighted gene co-expression network analysis (WGCNA). WGCNA is a comprehensive biological approach widely employed to analyze genetic association patterns across diverse samples, which is particularly effective for the identification of highly co-expressed genes. By examining the interrelatedness of genes and their associations with phenotypic traits, WGCNA facilitates the identification of potential candidate markers (28). Using the WGCNA R package (<http://www.genetics.ucla.edu/labs/horvath/CoexpressionNetwork/Rpackages/WGCNA/Tutorials/index.html>), a gene co-expression network for PCD was developed. The selection of the soft threshold power was performed using

the `pickSoftThreshold` function within the WGCNA package. Pearson's correlation analysis was then performed to evaluate the relationships between the LUAD index and module eigen-genes. The maximum Pearson correlation coefficient was used to identify the key module most closely correlated with the LUAD index. Genes intersecting within this module were considered candidate hub genes relevant to PCD in LUAD. To further investigate the relationships among PRGs, Spearman's correlation analysis was conducted. Protein-protein interactions (PPIs) of PCD-related proteins were investigated using the STRING database (<https://string-db.org/>), resulting in the establishment of a PPI network. Critical modules and hub genes were identified using the `cytohubba` and `MCODE` plugins in `Cytoscape 3.9.1` (<https://cytoscape.org/>). In addition, Gene Ontology (GO; <https://geneontology.org/>) and Kyoto Encyclopedia of Genes and Genomes (KEGG; <https://www.kegg.jp>) pathway analyses were performed to functionally annotate the PRGs.

Evaluation and verification of the prognostic significance of PRGs in patients with LUAD. The associations between the PRGs and overall survival (OS) were assessed using univariate Cox regression analysis. To refine the selection of candidate genes and construct a prognostic model, the least absolute shrinkage and selection operator (LASSO) regression algorithm was employed via the R package `glmnet` (<https://rdocumentation.org/packages/glmnet/versions/4.1-7>). Ultimately, six genes, along with their associated coefficients, were retained, with the penalty parameter (λ) selected based on the minimum criteria. The risk score was calculated by multiplying the gene expression levels obtained from the LASSO Cox regression model by their corresponding coefficients. This risk score was then applied to classify the patients with LUAD into high- and low-risk groups. Kaplan-Meier survival analysis was performed to compare the OS probability between these groups, and receiver operating characteristic (ROC) curve analysis was conducted using the `survminer` (<https://rdocumentation.org/packages/survminer/versions/0.4.9>), `timeROC` (<https://rdocumentation.org/packages/timeROC/versions/0.4>) and `survival` (version 2.41-0; <https://github.com/therneau/survival>) R packages. In addition, relevant clinical variables across different risk groups were compared using the χ^2 test, and the results were visualized as a heatmap.

To validate the prognostic signature, the aforementioned GSE8894, GSE31201, GSE30219 and GSE42127 GEO datasets were used. Univariate and multivariate Cox regression analyses were conducted using the `survivalROC` and `survival` R packages to evaluate whether the risk score served as an independent prognostic indicator. In addition, prognostic nomograms were developed using the `rms` (<https://rdocumentation.org/packages/rms/versions/6.5-0>) R package, incorporating risk scores and clinical stage to predict the OS of patients with LUAD. Calibration plots were constructed to evaluate the concordance between the predicted and observed 1-, 2-, 3- and 5-year OS rates.

Gene set enrichment analysis (GSEA) based on the signature. GSEA was employed to identify potential mechanisms by analyzing the enriched pathways in the low- and high-risk groups. The reference gene sets included HALLMARK,

C2:KEGG and C5:GO. The criteria for examination were a normalized enrichment score >1 , q -value <0.25 , and nominal P -value <0.05 .

Immune landscape analysis. The profiles of immune components were assessed using several algorithms, including QUANTISEQ, TIMER, XCELL, EPIC, MCPcounter and CIBERSORT, with visualization facilitated by the `limma` R (<https://rdocumentation.org/packages/limma/versions/3.28.14>) package. Gene set variation analysis and single-sample GSEA (ssGSEA) were employed to evaluate immune function and immune cell subset infiltration. The ESTIMATE algorithm was utilized to calculate stromal, immune and tumor purity scores on the basis of the proportions of stromal and immune cells. Additionally, the expression of major histocompatibility complex (MHC) molecules was analyzed using specific signatures. Differentially expressed common immune checkpoints, including members of the tumor necrosis factor receptor superfamily, programmed cell death protein 1 (PD-1), cytotoxic T lymphocyte-associated protein 4 (CTLA4), programmed cell death ligand 1 (PD-L1) and T-cell immune receptor with immunoglobulin and immunoreceptor tyrosine-based inhibitory motif domains, were visualized using boxplots. The tumor immune dysfunction and exclusion (TIDE) database (tide.dfci.harvard.edu/) was used to calculate TIDE scores, which predict the response to immune checkpoint inhibitor therapies, for patients with LUAD in TCGA dataset. For single-cell analysis, `t-distributed stochastic neighbor embedding` was employed to visualize the expression of six signature DRGs within the TME. Single-cell sequencing aids in the identification of specific gene expression patterns across distinct cell populations, thereby enhancing our understanding of the functions of prognostic genes in different cell types. Subsequently, the correlations of the six DRGs with various immune cell interactions were analyzed, including B cells, T cells, natural killer (NK) cells, monocytes, macrophages, dendritic cells (DCs) and neutrophils, using the `tidyverse` R package. These immune cells were further categorized into naive, memory, activated and resting states. To investigate the impact of varying levels of BDNF gene expression on the response of patients with lung cancer to immune checkpoint inhibitor therapy, four cohorts of patients with NSCLC treated with PD-1/PD-L1 inhibitor were analyzed, including patients undergoing systemic therapy and neoadjuvant therapy: GSE207422 (29), GSE111414 (30), GSE126044 (31) and GSE135222 (32).

Analysis of malignancy characteristics across different risk groups. Stemness, epithelial-mesenchymal transition (EMT), angiogenic activity and tumorigenic cytokines serve as crucial indicators of malignant tumor properties. Scores for these characteristics in every tumor sample were calculated using the ssGSEA algorithm. Tumor stemness indices (TSIs) for patients diagnosed with LUAD were obtained from prior research (33), which identified that TSIs correlate with higher levels of tumor dedifferentiation and the presence of tumor stem cells. Somatic mutation data were obtained from TCGA, and gene mutation analysis was conducted employing the `maftools` R package. The tumor mutation burden (TMB) was computed for every patient and compared between the two risk groups. TMB score-based survival analysis was also

performed. The cBioPortal for Cancer Genomics database (<http://www.cbioportal.org/>) was adopted to visualize somatic mutations in the key DRG signature.

Potential drug prediction. The limma R package was used to detect differentially expressed genes between the two risk groups, which were subsequently used for small-molecule drug screening. The list of differentially expressed genes was submitted to the Connectivity Map database (CMap; <https://clue.io/>) to identify potential compounds relevant to the six-gene signature. The CMap database features gene expression profiles derived from nine cancer cell lines treated with 2,429 compounds, each with detailed annotations (34). Connectivity scores were calculated by matching CMap data with the expression levels of the six signature genes, in which these scores were negatively correlated with the treatment effects of the compounds. The pRRophetic (<https://github.com/paulgeeleher/pRRophetic2>) R package was also used to predict the half-maximal inhibitory concentration (IC₅₀) values for standard chemotherapeutics in different risk subgroups. Subsequently, the three-dimensional structures of potential therapeutic compounds were retrieved from the PubChem database (<https://pubchem.ncbi.nlm.nih.gov/>).

Sulforhodamine B assays. Given the limited research on the role of honokiol in inducing PCD in lung adenocarcinoma and as honokiol was among the top 10 drugs identified by CMap with the highest enrichment scores, this compound was selected for further study. A549 cells were treated with honokiol, and sulforhodamine B (SRB) assays along with JC-1 staining were performed to validate the predictive accuracy of the CMap drug analysis. Honokiol and Taxol were obtained from Selleck Chemicals. For the SRB assay, A549 cells were seeded at a density of 8,000 cells per well in 96-well plates and incubated under standard conditions (37°C in 5% CO₂) for 24 h. Honokiol (0, 20, 40, 60 or 80 μM) and Taxol (0, 20, 40, 60 or 80 nM) were added to the treatment groups. Following 24 and 48 h of incubation, the SRB method was used to evaluate cell viability.

JC-1 staining assays. A549 cells were seeded into 6-well plates at a density of 1x10⁶ cells per well and subjected to the following treatments to form groups: Control (DMEM only), honokiol (50 μM), Taxol (50 nM), and a combination of honokiol (50 μM) + Taxol (50 nM). The cells were incubated at 37°C with 5% CO₂ for 24 h. Subsequently, staining was performed following the instructions provided with the JC-1 assay kit (IJ03009; Beijing Solarbio Science & Technology Co., Ltd.). Fluorescence images were captured using a fluorescence microscope (Axio Observer A1; Zeiss AG), and the fluorescence intensity ratio was quantified using ImageJ v1.8.0 (National Institutes of Health).

Validation of the protein expression of the six prognosis-relevant genes. Immunohistochemistry data from the Human Protein Atlas (HPA; <http://www.proteinatlas.org/>) were used to validate the expression of the proteins corresponding to the prognostic genes in LUAD samples compared with normal lung samples.

MR. Two-sample MR was employed to investigate the relationship between the risk of LUAD and hub genes, with single nucleotide polymorphisms (SNPs) defined as instrumental variables (IVs). Hub gene data were sourced from the Genome Wide Association Study database (<https://gwas.mrcieu.ac.uk/>). The core gene BDNF (id: prot-a-2122), and LUAD (id: ebi-a-GCST004744, containing 11,273 LUAD samples, 55,483 normal samples and 7,849,324 SNPs) as the representative disease, were selected for MR analysis. The analysis was conducted using the TwoSampleMR package, with inverse variance weighting (IVW) to evaluate the association between the hub gene expression value and the risk of LUAD. The MR-Egger method was applied for extra sensitivity analysis.

Cell culture and preparation of BDNF knockdown Lewis lung carcinoma (LLC) cells. The lung cancer A549 (CCL-185TM), LLC (CRL-1642TM) and H1975 (CRL-5908TM) cell lines, and the normal human bronchial epithelial BEAS-2B (CRL-9609TM) cell line were purchased from the American Type Culture Collection. These cells were cultured in DMEM (C11875500BT; Gibco; Thermo Fisher Scientific, Inc.) into which 1% penicillin-streptomycin (15070063; Gibco; Thermo Fisher Scientific, Inc.) and 10% fetal bovine serum (10099-141; Gibco; Thermo Fisher Scientific, Inc.) were added. The cells were kept in an incubator at 37°C with 5% CO₂.

The small interfering RNA (siRNA) sequences and expression plasmids were designed and synthesized by Guangzhou RiboBio Co., Ltd. Specific siRNAs targeting BDNF (siBDNF-1 sense, 5'-TCCTTTTCCTTACTATGGTTATT-3' and antisense, 5'-AAUAACCAUACUAAGGAAAAGGA-3'; and siBDNF-2 sense, 5'-TTCCTTACTATGGTTATTTTCATA-3' and antisense, 5'-UAUGAAUAACCAUAGUAAGGAA-3') and control siRNA (sense, 5'-TCCCAAATCGTCTGACCGATGATCCGT TCAAGAGACGGATCATCGGTCAGACGATTTT-3' and antisense, 5'-AAA AUCGUCUGACCGAUGAUCGUCUC UGAACGGAUCAUCGGUCAGACGAUUUGGGA-3') were purchased from Santa Cruz Biotechnology, Inc. Prior to transfection, LLC cells were plated into 6-well culture plates and allowed to grow until reaching 70-80% confluence within 24 h. According to the manufacturer's protocol, siRNA transfection was performed using Lipofectamine[®] 3000 (Invitrogen; Thermo Fisher Scientific, Inc.) and siRNAs (50 nM). The transfection process was maintained in an incubator (37°C, 5% CO₂) for 8 h, after which the medium was replaced with fresh complete medium for an additional 48 h of incubation. Subsequently, the cells were harvested for further experiments.

Reverse transcription-quantitative polymerase chain reaction (RT-qPCR). Total RNA was isolated from the cell lines using TRIzol[®] reagent (cat. no. 15596-026; Ambion; Thermo Fisher Scientific, Inc.). Total RNA was isolated from A549, LLC and BEAS-2B cells. The RNA purity and concentration were measured according to the ratio of absorbance at 260 and 280 nm, using a NanoDrop spectrophotometer (Thermo Fisher Scientific, Inc.). The RNA was then reverse-transcribed into cDNA using the PrimeScript[®] RT reagent (Takara Bio, Inc.) according to the manufacturer's protocol. The thermocycling protocol was as follows: Amplification step, 94°C for 5 min; followed by 35 cycles of denaturation for 1 min at 94°C, 1 min of annealing at 55°C, elongation at 72°C for 1 min and a final

extension step at 72°C for 1 min. The cDNA then served as the template for qPCR, with β -actin as the reference gene. Standard two-step qPCR amplification was conducted using SYBR Green I (10222ES60; Shanghai Yeasen Biotechnology Co., Ltd.) according to the manufacturer's protocol. A total of 20 μ l qPCR reaction system contained 6 μ l nuclease-free water, 10 μ l SYBR Premix Ex Taq II (2X), 0.4 μ l ROX Reference Dye II, 2 μ l cDNA, 0.8 μ l forward primer (10 μ M) and 0.8 μ l reverse primer (10 μ M). The thermocycling conditions were as follows: 95°C for 30 sec; followed by 40 cycles of denaturation at 95°C for 5 sec, annealing at 60°C for 34 sec, elongation at 95°C for 15 sec, and extension at 60°C for 1 min. Gene expression levels were calculated using the $2^{-\Delta\Delta C_q}$ method (35). The primers used are listed in Table SII.

Wound healing and colony formation assay. For the colony formation assay, transfected cells in the logarithmic growth phase were seeded at a density of 1,000 cells/well into a 6-well plate. After cultivation for 10 days (37°C in 5% CO₂), the cells were fixed with methanol for 20 min at room temperature, and then stained with 0.1% crystal violet for 15 min at room temperature. Images of the colonies formed in each well were captured and the number of colonies was manually counted. In this study, clusters of cells containing >50 cells were considered colonies. For the wound healing assay, transfected cells were seeded at a density of 2x10⁵ cells/well in a 6-well plate. After incubation for 24 h, a scratch tool was used to form a wound in the cell monolayer, and the medium was then replaced with serum-free medium. Images of the wound were captured at 0 h and 48 h using a light microscope. ImageJ v1.8.0 (National Institutes of Health) was used to evaluate the cell migration rate as follows: Wound closure surface area / wound total surface area x100.

Western blotting. Total cellular proteins were extracted from transfected cells using RIPA lysis buffer, and their concentrations were measured with the Thermo BCA Protein Assay kit (Thermo Fisher Scientific, Inc.). The proteins were subsequently denatured at 95°C for 5 min in a water bath, separated on a 10% SDS-PAGE gel by electrophoresis, and transferred onto a 0.45- μ m PVDF membrane. The membrane was then blocked with 5% skimmed milk at room temperature for 1 h, followed by the addition of primary antibody (pRIPK1, 1:1,000, cat. no. HY-p81539, MedChemExpress; RIPK1, 1:1,000, cat. no. 3493T, Cell Signaling Technology, Inc.; Cleaved CASP8, 1:1,000, cat. no. 8592T, Cell Signaling Technology, Inc.; CASP8, 1:1,000, cat. no. 4790T, Cell Signaling Technology, Inc.; Cleaved CASP1, 1:1,000, cat. no. HY-p80587, MedChemExpress; CASP1, 1:1,000, cat. no. HY-p81232, Cell Signaling Technology, Inc.; β -actin, 1:2,000, cat. no. 81115-1, Proteintech Group, Inc.) and incubation at 4°C overnight. After washing with TBST, the membrane was incubated with secondary antibody (anti-rabbit IgG, HRP-linked antibody, 1:3,000, cat. no. 7074P2, Cell Signaling Technology, Inc.) for 1 h at room temperature and washed again with TBST. Finally, a chemiluminescence reagent (Shanghai Biyuntian Biotechnology Co., Ltd.) was applied, and the membranes were developed using an automatic chemiluminescence imaging system (Odyssey; LI-COR Biotechnology).

Statistical methods. All data were statistically analyzed using R software (version 4.2.1; www.r-project.org) with a two-tailed P-value of <0.05 considered to indicate a statistically significant difference. Kaplan-Meier analysis and log-rank test were conducted to compare the OS of the groups. Independent predictors were examined using Cox regression analysis. Hazard ratios (HRs) and 95% confidence intervals (CIs) were used to describe relative risk. Correlation analyses were performed using Spearman's method. Categorical variables of clinical factors (sex, stage, age and TNM status) were analyzed using the χ^2 test or Fisher's exact test. Student's t-test was used to compare two groups of normally distributed data, while ANOVA with Tukey's post hoc test was employed for multiple-group comparisons. Wilcoxon's test was employed for comparing ordinal and non-normally distributed data between subgroups. Data from cellular experiments were processed using GraphPad Prism 7.0 software (Dotmatics). The data are expressed as the mean \pm SD from a minimum of three replicates.

Results

Detection of differentially expressed PRGs in LUAD. Differential expression of the 1,670 PRGs identified from TCGA was analyzed between LUAD samples (n=412) and adjacent normal tissues (n=43). The volcano plot (Fig. 1A) and heatmap (Fig. 1B) demonstrated that 310 PRGs were significantly differentially expressed between the LUAD and normal tissues.

Construction of WGCNA network and identification of PCD-related module in LUAD. To determine the association between potential gene modules and LUAD, a WGCNA was performed on all candidate genes from the LUAD dataset from TCGA. The WGCNA R package was used to develop a system with the optimum efficacy value ($\beta=3$, $R^2=0.9$; Fig. 1C and D). The 1,670 PRGs were grouped into seven modules based on their co-expression patterns, including the gray module. The clustering analysis results for all samples are shown in Fig. 1E, and the co-expression modules are visually represented in Fig. 1F using different colors. The results of the module correlation analysis indicate that the yellow module is the most strongly correlated with LUAD ($r=-0.85$; $P<0.0001$).

GO/KEGG enrichment analyses and PPI network analysis for core genes. To determine the core differentially expressed PRGs in LUAD, the 310 differentially expressed genes from TCGA and the yellow module (150 genes) from the WGCNA analysis were imported into a Venn diagram. There were 84 overlapping genes that were identified as core genes for subsequent analysis (Fig. 2A). Subsequently, the differentially expressed genes were subjected to GO and KEGG pathway enrichment analyses. The GO analyses revealed that the genes were predominantly enriched in 'cellular response to interleukin-1', 'cellular response to tumor necrosis factor', 'inflammatory response', 'apoptotic process' and 'positive regulation of apoptotic process' (Fig. 2B). The KEGG analyses revealed that the genes were predominantly enriched in 'PI3K-Akt signaling pathway', 'IL-17 signaling pathway',

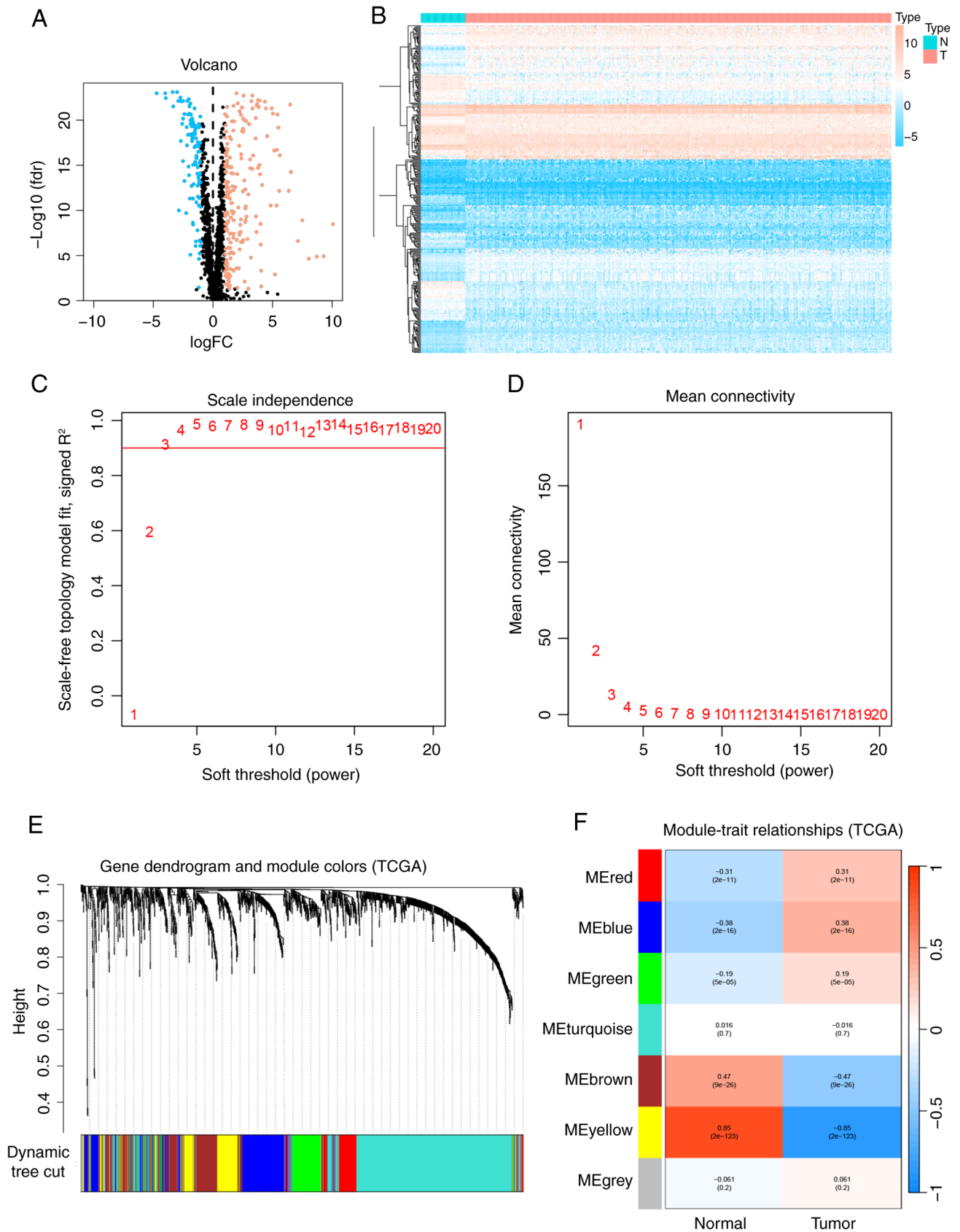


Figure 1. WGCNA and differential gene expression analysis between LUAD and normal samples. (A) Volcano plot illustrating the differential expression analysis of TCGA data. (B) Heatmap depicting the differential expression analysis of TCGA data. Blue indicates downregulated genes, red indicates upregulated genes and black denotes genes without significantly differential expression. (C) Scale independence analysis and (D) mean connectivity analysis conducted using WGCNA. (E) Dendrogram showing the clustering of all genes in TCGA data, based on a topological overlap matrix (1-TOM). Each branch in the dendrogram corresponds to a gene, and different colors represent distinct co-expression modules. (F) Module-trait heatmap displaying the correlation between gene modules and LUAD within TCGA data, with correlation coefficients (above) and P-values (below) indicated for each module. LUAD, lung adenocarcinoma; TCGA, The Cancer Genome Atlas; WGCNA, weighted gene co-expression network analysis; fdr, false discovery rate; FC, fold change; N, normal samples; T, tumor samples; ME, module eigengene.

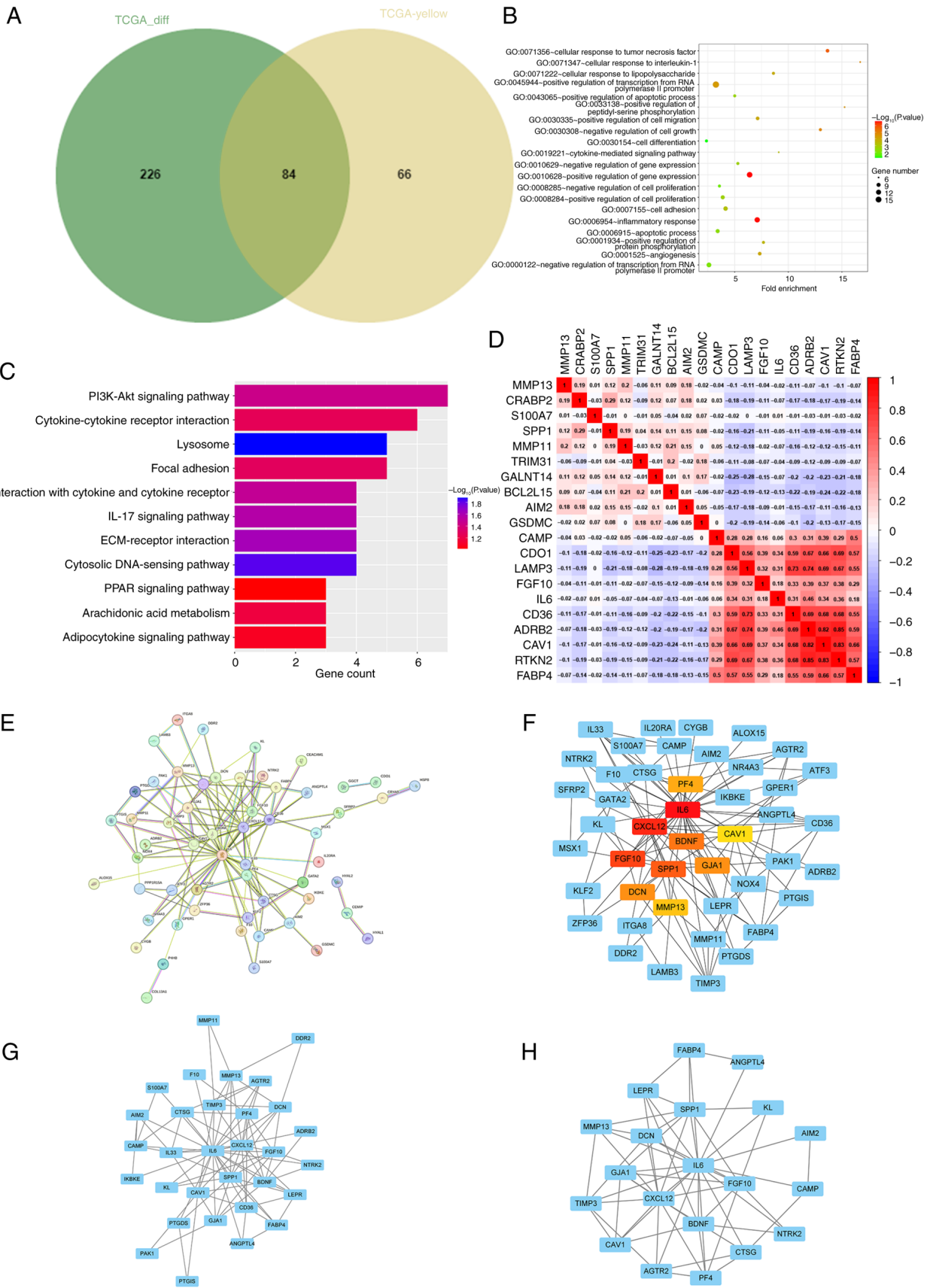


Figure 2. Screening and validation of candidate hub genes. (A) Venn diagram showing 84 candidate hub genes shared between the differentially expressed PRGs and the yellow module from the weighted gene co-expression network analysis. (B) GO enrichment analysis of PRGs. (C) Kyoto Encyclopedia of Genes and Genomes enrichment analysis of PRGs. (D) Spearman correlation analysis of 20 differentially expressed PRGs in lung adenocarcinoma, with red squares denoting positive correlations and blue squares indicating negative correlations. (E) Full PPI network and (F) the 10 key hub genes visualized in a PPI network using the cytohubba plugin of Cytoscape, where increased redness signifies a gene with a higher number of direct connections. (G and H) Two modules identified using the MCODE plugin of Cytoscape. GO, Gene Ontology; PRGs, programmed cell death-related genes; PPI, protein-protein interaction; TCGA, The Cancer Genome Atlas.

'ECM-receptor interaction', 'Cytokine-cytokine receptor interaction' and 'PPAR signaling pathway' (Fig. 2C). Correlations between the downregulated and upregulated genes are illustrated in Fig. 2D. A PPI network was then constructed utilizing Cytoscape software in conjunction with the STRING database (Fig. 2E). From this network, the top 10 hub genes were identified through degree analysis. These were PF4, IL6, CXCL12, BDNF, CAV1, FGF10, SPP1, GJA1, DCN and MMP13, as shown in Fig. 2F (colored nodes). Additionally, two modules were identified using the MCODE plugin (Fig. 2G and H).

Six-gene risk signature independently predicts outcome in patients with LUAD. Considering the association between PCD regulators and OS in patients with LUAD, univariate Cox regression analysis was conducted on the expression levels of 84 PRGs to assess their clinical relevance, and the top 20 PRGs with hazard ratios are displayed in a forest chart. The analysis revealed that adrenergic receptor b2 (ADRB2), microtubule associated protein 6 (MAP6) and recombinant integrin $\alpha 8$ functioned as protective factors, while BDNF, G protein-coupled estrogen receptor 1 (GPER1), angiopoietin-like protein 4 (ANGPTL4) and laminin b3 (LAMB3) were identified as risk factors (Fig. 3A). Additionally, correlation analyses showed that most of these protective and risk factor genes were interrelated (Fig. 3B).

To examine the clinical relevance of the PRGs further, patients with LUAD were grouped into subcategories according to their gene expression profiles. Optimal clustering was achieved with $k=2$, resulting in the separation of the patients into two distinct and non-overlapping groups (Figs. 3C-E). Significant variations in OS, age, stage and sex between these clusters were then assessed. The results indicated that patients in cluster 1 had an improved prognosis ($P=0.003$) compared with that of patients in cluster 2 (Fig. 3G). Additionally, cluster 1 exhibited lower N stages compared with cluster 2 (Fig. 3F). In summary, consensus clustering revealed a notable association between PRG expression patterns and different clinical parameters.

LASSO Cox regression analysis indicated that *BDNF*, *GPER1*, *ANGPTL4* and *LAMB3* have the highest predictive capabilities (Fig. 3H), as these were risk genes with $HR \geq 1$. By contrast, *ADRB2* and *MAP6* were protective genes with $HR < 1$. In addition, the LASSO Cox regression analysis identified six genes with the highest predictive power (Fig. 3I and J). By utilizing the coefficients derived from the LASSO algorithm, six optimal genes, namely *BDNF*, *GPER1*, *ANGPTL4*, *LAMB3*, *ADRB2* and *MAP6*, were used to construct the risk model (Fig. 3K). Accordingly, the risk score derived from these coefficients may be calculated as follows: Risk score = $(0.224877 \times \text{expression level of } BDNF) + (0.060886 \times \text{expression level of } GPER1) - (0.08495 \times \text{expression level of } ADRB2) - (0.17324 \times \text{expression level of } MAP6) - (0.005609 \times \text{expression level of } ANGPTL4) - 0.002494 \times \text{expression level of } LAMB3$. The associations between the risk score and the six genes are illustrated in Fig. 3L.

To assess the survival prediction value of these gene signature models, patients with LUAD were categorized into low- and high-risk groups according to the median risk score. A heatmap of clinically relevant characteristics was created to illustrate the differential expression of the six prognostic PRGs

between the high- and low-risk groups (Fig. 4A). Significant variations in the clinical data were observed for sex ($P < 0.001$), follow-up status ($P < 0.001$), stage ($P < 0.05$), lymph node metastasis ($P < 0.001$) and tumor extent ($P < 0.01$). Cox univariate analysis revealed that risk scores, tumor stage, tumor extent and lymph node metastasis were significantly associated with OS in patients with LUAD ($P < 0.001$; Fig. 4B). Multivariate Cox regression analysis was then conducted to evaluate whether the risk score independently predicts OS in patients with LUAD, independent of other clinicopathological characteristics. The results demonstrated that the risk score ($P < 0.001$), stage ($P = 0.008$), and M stage ($P = 0.043$) were independently associated with OS ($P < 0.001$; Fig. 4C). In summary, the six-gene risk signature predicts the prognosis of patients with LUAD independently of other clinicopathological factors, including grade, histological age, sex and TNM stage.

Survival analysis and ROC curve evaluation using the prognostic model. Survival analyses were conducted using data from 371 patients with LUAD from TCGA, and the results showed that the OS of high-risk patients was significantly poorer compared with that of patients in the low-risk group ($P < 0.001$; Fig. 4D). The 5-year OS rates were 48.3% for the low-risk group and 24.5% for the high-risk group. ROC curve analysis demonstrated that the area under the curve (AUC) for 1-, 3- and 5-year OS was 0.719, 0.712 and 0.628, respectively, indicating a strong predictive power for clinical outcomes. In addition, the distribution of risk scores among the patients with LUAD was determined, and survival status illustrated utilizing a dot matrix (Fig. S1).

The predictive capacity of the risk model was assessed in four GEO datasets for validation. Patients in the cohorts were classified into low- and high-risk groups based on the cutoff value of TCGA cohort. Survival analysis outcomes indicated that the low-risk group experienced significantly improved OS (GSE8894, $P = 0.033$; GSE31201, $P < 0.001$; GSE30219, $P = 0.011$; and GSE42127, $P = 0.01$) compared with that of the high-risk group (Figs. 4E-H). This finding is consistent with the results observed in TCGA cohort. The AUC for 1-year OS ranged from 0.566 to 0.719, for 3-year OS from 0.652 to 0.741 and for 5-year OS from 0.642 to 0.705. These findings validate the predictive accuracy of the risk model (Figs. 4E-H). Analysis of risk scores among various clinicopathological factors revealed that patients who died had a higher risk score than those who survived ($P = 0.044$), and patients with more advanced disease, those with T2-4 tumors ($P = 0.0003$), N1-3 status ($P = 0.0001$) and stage II-IV ($P = 0.002$), had higher risk scores. Consequently, higher risk scores were found to be associated with more advanced tumor stages (Fig. 4I).

Construction of a nomogram. To support the clinical implementation of the model, a comprehensive prognostic nomogram was developed incorporating the LUAD stage and risk score (Fig. 5A). This nomogram effectively predicted the 1-, 3- and 5-year OS of patients with LUAD. The AUC for the risk score was 0.742, indicating a strong association between the predictive effectiveness of the model and the tumor stage (Fig. 5B). These results confirm the good predictive value of the model for patients with LUAD. Calibration plots indicated

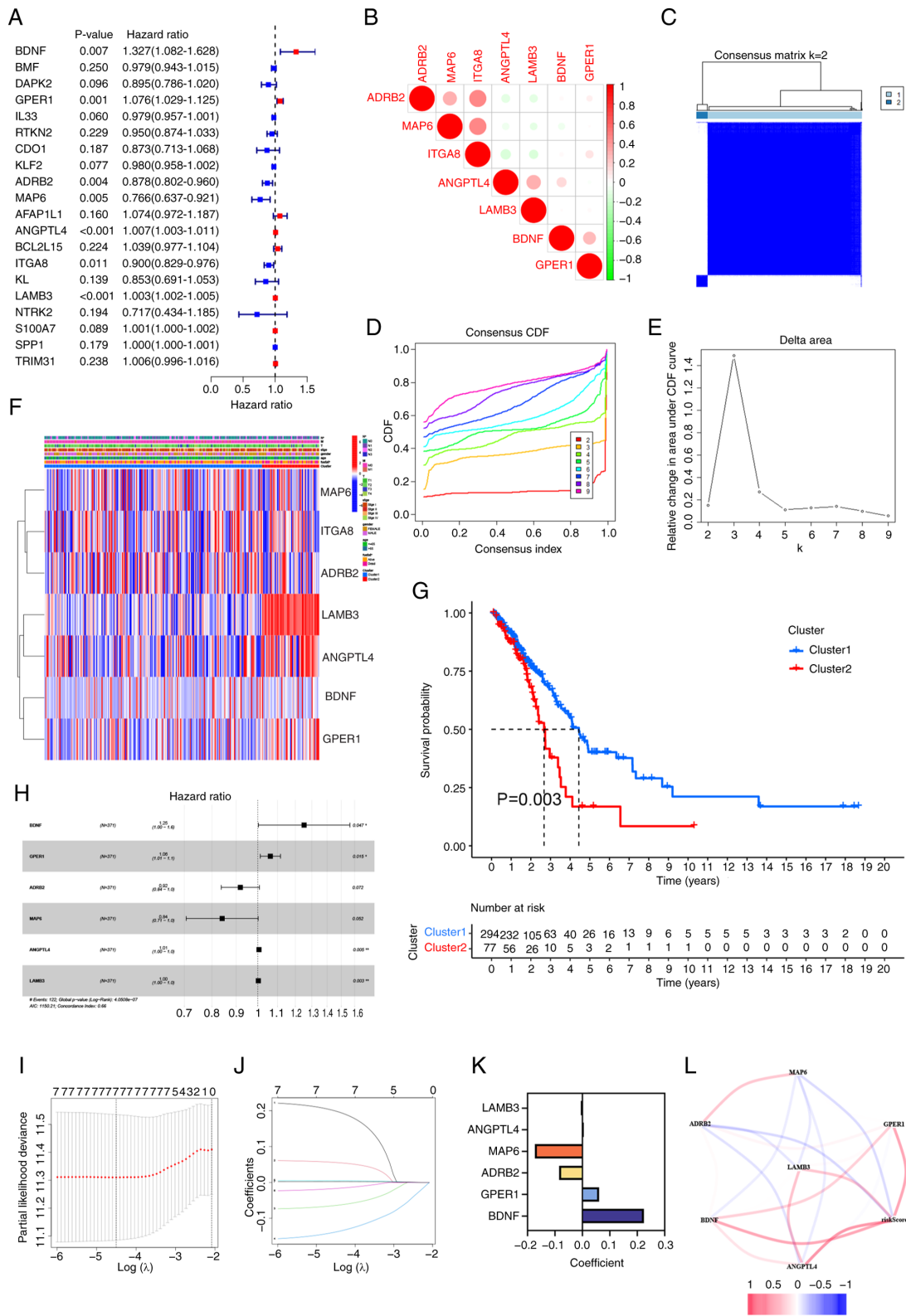


Figure 3. Two clusters of PRGs can predict OS in lung adenocarcinoma and establishment of a prognostic risk model. (A) Forest plot illustrating the results of univariate Cox regression analysis for 20 PRGs. (B) Correlation matrix of signature PRGs. (C) Cluster analysis showing the correlation between subgroups with k=2 clusters. (D) CDF plot for cluster numbers k=2-9. (E) Relative change in the area under the CDF curve for k=2-9. (F) Heatmap displaying the clinicopathological features and gene expression levels of the two clusters, with blue indicating low expression and red indicating high expression. (G) Comparison of OS between the two clusters. (H) Univariate Cox regression analysis of the six key PRGs: BDNF, GPER1, ADRB2, MAP6, ANGPTL4 and LAMB3. (I) The cross-validation curve of the seven prognosis-related PRGs. The X-axis represents the logarithm of the penalty coefficient, $\log(\lambda)$, while the Y-axis denotes the likelihood deviance. The left dashed line indicates λ min, representing the λ value at which the model achieves the best fit. (J) The LASSO coefficient path plot of the seven prognosis-related PRGs. Each curve represents the trajectory of changes in the coefficient of each variable. The vertical axis indicates the coefficient values, the lower horizontal axis corresponds to $\log(\lambda)$, and the upper horizontal axis shows the number of non-zero coefficients in the model at that point. (K) Correlation coefficients of the six PRGs incorporated into the prognostic signature. (L) Correlations among the prognostic genes. PRGs, programmed cell death-related genes; OS, overall survival; CDF, cumulative distribution function; BDNF, brain-derived neurotrophic factor; GPER1, G protein-coupled estrogen receptor 1; ADRB2, adrenergic receptor b2; MAP6, microtubule associated protein 6; ANGPTL4, angiopoietin-like protein 4; LAMB3, laminin b3.

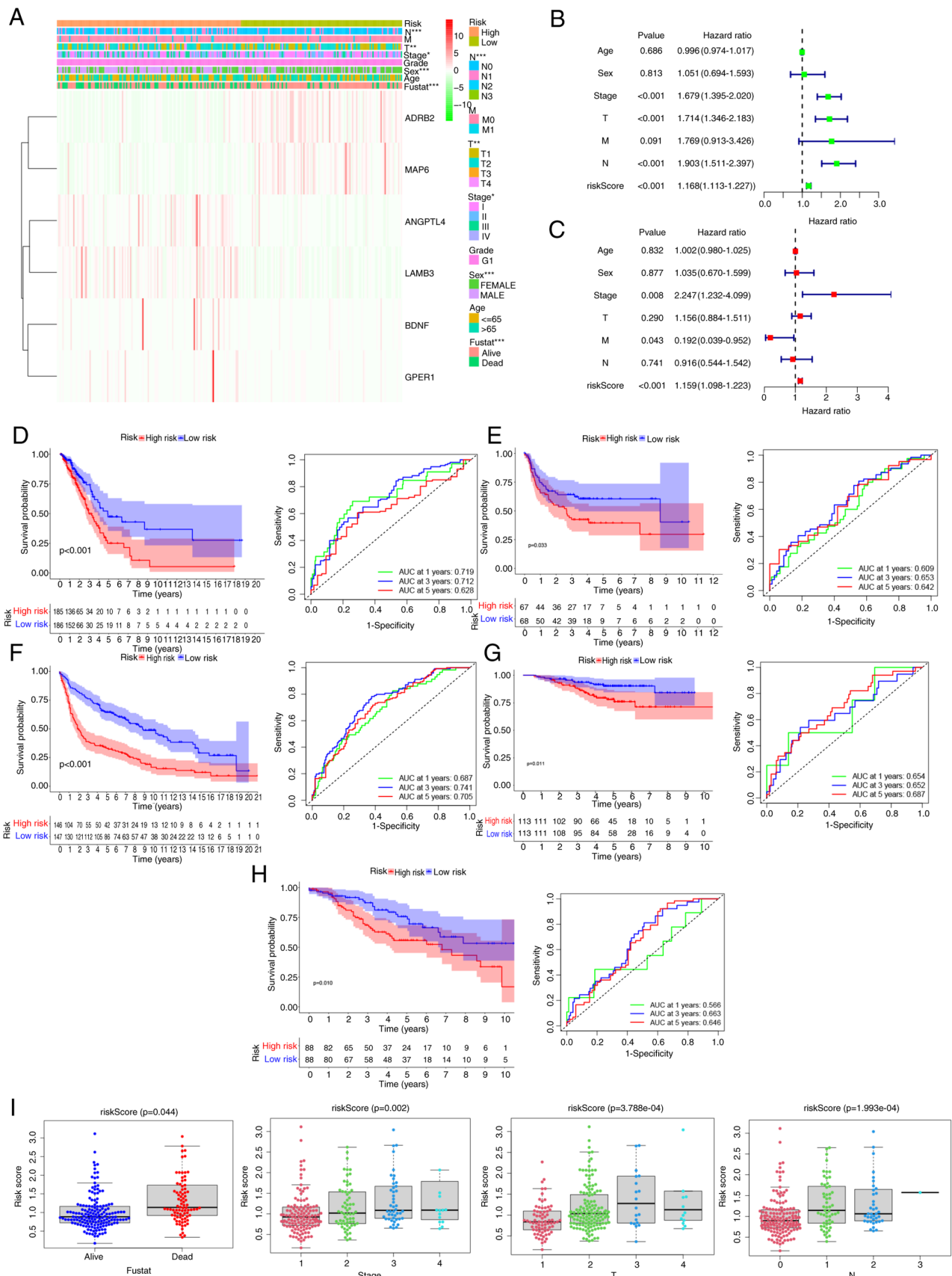


Figure 4. Performance validation of the prognostic model. (A) Heatmap illustrating the expression levels of the six programmed cell death-related genes and distribution of clinicopathological features in two risk populations. (B) Univariate and (C) multivariate Cox regression analysis of clinicopathological factors and overall survival. (D) Analysis of survival curves (left panel) and ROC curves (right panel) for The Cancer Genome Atlas cohort. Survival curves (left panel) and ROC curves (right panel) for the (E) GSE8894, (F) GSE31201, (G) GSE30219 and (H) GSE42127 datasets. (I) Variations in risk scores among subgroups with differing clinicopathological factors. ROC, receiver operating characteristic; fustat, follow-up stage; AUC, area under the curve; BDNF, brain-derived neurotrophic factor; GPER1, G protein-coupled estrogen receptor 1; ADRB2, adrenergic receptor b2; MAP6, microtubule associated protein 6; ANGPTL4, angiopoietin-like protein 4; LAMB3, laminin b3.

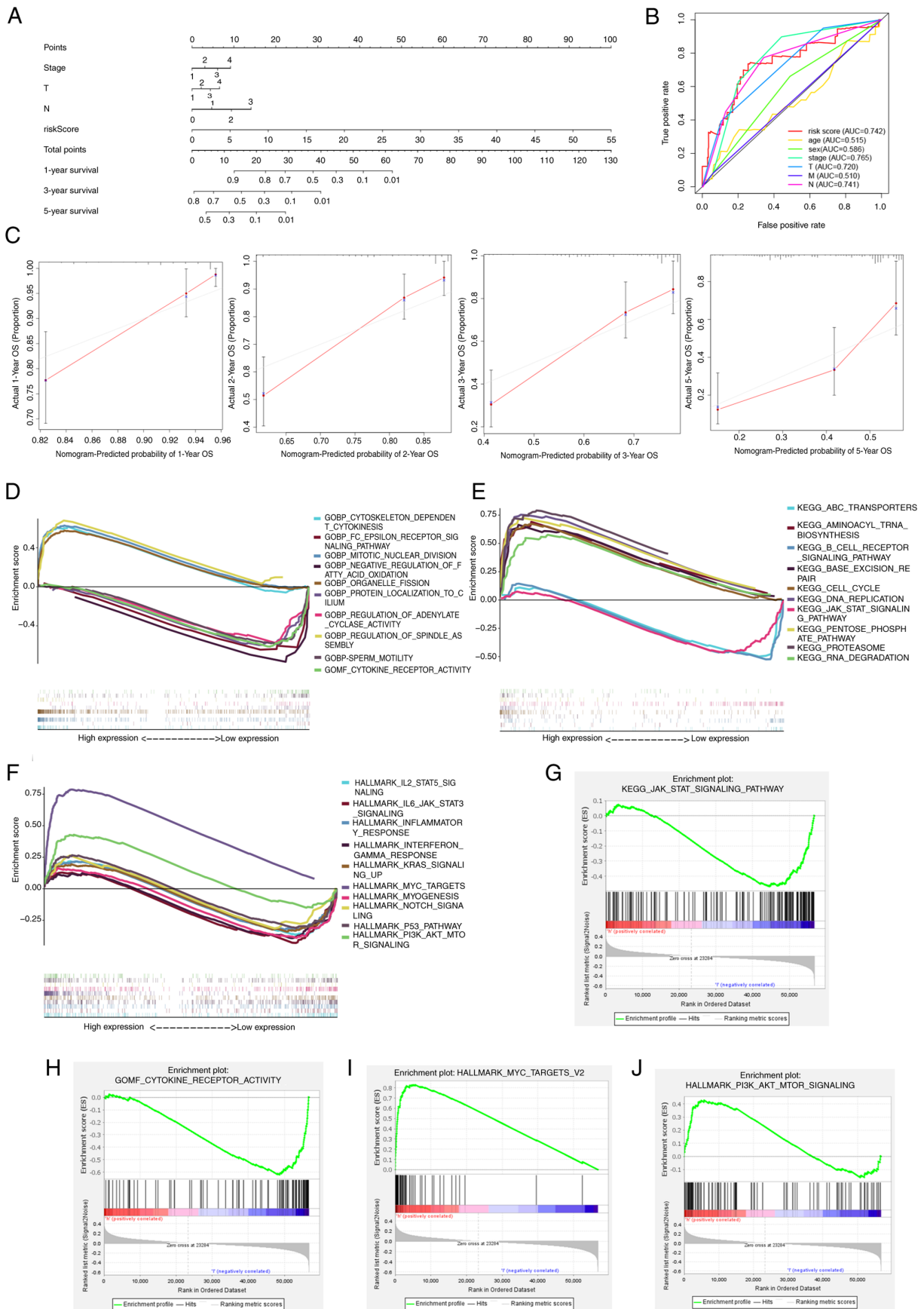


Figure 5. Development of a nomogram and functional enrichment analysis for six programmed cell death-related genes. (A) Integration of clinical data with prognostic nomograms for the prediction of the 1-, 3- and 5-year OS of patients with lung adenocarcinoma. (B) Evaluation of the predictive performance of the model using receiver operative characteristic curves. (C) Calibration plots of the nomogram for the prediction of 1-, 2-, 3- and 5-year OS probabilities. Gene set enrichment analysis using (D) GO, (E) KEGG and (F) HALLMARK databases. Comparison of the low- and high-risk groups reveals that (G) ‘JAK-STAT signaling pathway’ and (H) ‘cytokine receptor activity’ are lower in the high-risk group, while (I) ‘MYC targets’ and (J) ‘PI3K-AKT-mTOR signaling’ are higher in the high-risk group. OS, overall survival; GO, Gene Ontology; KEGG, Kyoto Encyclopedia of Genes and Genomes; AUC, area under the curve.

a strong agreement between the actual and predicted survival rates at 1-, 2-, 3- and 5- years (Fig. 5C).

Biological functional enrichment analysis of prognostic signature of PRGs. Enrichment analyses were performed using GO (Fig. 5D), KEGG (Fig. 5E) and HALLMARK (Fig. 5F) databases to identify PRGs with differential expression between the high- and low-risk groups and to explore subgroup survival benefits associated with biological processes and signal pathways. The analyses revealed that high-risk groups were associated with weaker immune response and inflammation-related functions, including ‘JAK-STAT signaling pathway’, ‘IL6-JAK-STAT signaling’, ‘cytokine receptor activity’, ‘inflammatory response’, ‘cytokine receptor activity’ and ‘interferon gamma response’. Conversely, cancer-promoting functions such as ‘DNA replication’, ‘MYC targets’ and ‘PI3K-AKT-MTOR signaling’ were upregulated in the high-risk group, indicating their association with worse prognosis. Selected results of the enrichment are depicted in Figs. 5G-J.

Correlation of immune infiltration and malignant features with prognosis-related PRGs. Functional enrichment analyses indicated that the primary roles of the PRGs encompass inflammation, immune response and PCD. Therefore, an immune infiltration analysis was performed to confirm these results. Using the CIBERSORT, MCPcounter, TIMER, QUANTISEQ, XCELL and EPIC algorithms, the levels of DCs ($P < 0.01$), CD8⁺ T cells (CIBERSORT, $P = 0.006$; and XCELL, $P = 0.003$), T-helper 1 (Th1) cells (XCELL, $P = 0.017$), NK (XCELL, $P < 0.001$) and B cell plasma (XCELL, $P = 0.016$) were observed to be lower in the high-risk group compared with those in the low-risk group. However, M2 macrophages (CIBERSORT, XCELL and QUANTISEQ, $P < 0.05$) and cancer-associated fibroblast (CAF) (MCPcounter and EPIC, $P < 0.05$) levels were revealed to be higher in the high-risk group than in the low-risk group (Fig. 6A and B). The difference in expression of these factors suggests that immune infiltration may influence patient prognosis. Moreover, the quantification of enrichment fractions suggests that reduced immune function may impact the prognosis of patients in the high-risk groups, due to an association with cytolytic activity ($P < 0.05$), C-C chemokine receptor ($P < 0.05$), human leukocyte antigen ($P < 0.001$), check-point ($P < 0.01$), T cell co-stimulation and interferon response ($P < 0.05$) (Fig. 6C). The ESTIMATE algorithm indicated higher tumor purity ($P < 0.001$), as well as lower immune ($P < 0.001$), ESTIMATE ($P < 0.001$) and stromal ($P < 0.001$) scores, in the high-risk group compared with the low-risk group (Fig. 6D). By contrast, the expression of MHC molecules was significantly higher in the low-risk group (Fig. 6E). Additionally, a distinct association was observed between the low-risk group and elevated expression of multiple immune checkpoints, such as TIGIT ($P < 0.01$), CD276 ($P < 0.001$), CTLA4 ($P < 0.01$) and CD244 ($P < 0.001$) (Fig. 6F), suggesting that these patients could be advantageously treated with immune checkpoint inhibitors. Notably, the low-risk group also exhibited higher tumor TIDE ($P < 0.001$) and M2 tumor-associated macrophage scores ($P = 0.004$), and lower levels of CAFs ($P = 0.004$) and myeloid-derived suppressor cells ($P < 0.001$) (Fig. 6G). Furthermore, lower TSIs,

including differentially methylated probes-based stemness index ($P = 0.016$), epiregulin-mDNA stemness index ($P < 0.001$), enhancer-based stemness index ($P = 0.004$) and mRNA stemness index ($P < 0.001$), were observed in the low-risk group (Fig. 6H). The high-risk group had a lower stemness score ($P = 0.014$) but a higher angiogenic activity score ($P < 0.001$) (Fig. 6I). No significant differences in tumorigenic cytokines or EMT scores were identified between the high- and low-risk groups. Moreover, assessment of the correlation of the risk score with malignant features (Fig. 6J) indicated that the risk score had an association with angiogenic activity score ($R = 0.35$, $P < 0.001$) and stemness score ($R = -0.15$, $P = 0.004$).

Single-cell analysis revealed limited expression of the six DRGs in immune cells (Fig. 7). For example, GPER1 exhibited low expression in CD8⁺ T cells, and ADRB2 was mainly expressed in macrophages, T cells and B cells, while LAMB3 exhibited slightly elevated expression in monocytes, NK cells and B cells. Combined with the previous immune infiltration analysis, these findings suggest that the six DRGs are primarily expressed in tumor cells and may serve as predictors for patient risk stratification. Further analysis of immune infiltration and single-gene associations (Fig. S2) revealed that BDNF expression was positively correlated with the mutual promotion of T cells CD4 memory activated, T cells CD8, macrophages and T cells CD4 memory activated. GPER1 expression was mainly positively correlated with the mutual promotion of monocytes and T cells CD4 memory resting, as well as mast cells resting and monocytes. ADRB2 was positively correlated with interactions between neutrophils and macrophages M2. MAP6 exhibited a positive correlation with the mutual promotion of monocytes, macrophages M2, DCs resting, DCs activated, mast cells resting and eosinophils. ANGPTL4 was positively correlated with the mutual promotion of mast cells activated, eosinophils and neutrophils. LAMB3 was positively correlated with interactions between T cells CD8, T cells CD4 memory activated and macrophages M1. These findings indicate that the expression of the six PRGs genes shows no significant variation in TME-associated immune cells, but is closely associated with immune cell function and interactions. Therefore, we hypothesize that PCD primarily occurs in tumor cells within the TME, which significantly promotes the activation and interactions of immune cells. This also suggests that the predictive model constructed in the present study not only estimates patient prognosis and risk stratification but also effectively reflects the immune functional status within the TME.

Four NSCLC immunotherapy cohorts were utilized to validate the impact of BDNF on the response to immune checkpoint inhibitors (Fig. S3). The results from the GSE135222 cohort indicated that patients with low BDNF expression treated with PD-1/PD-L1 inhibitors experienced improved progression-free survival compared with those patients with high BDNF expression ($P < 0.001$; Fig. S3A). The findings from the GSE126044 cohort revealed that patients whose lung cancer was more sensitive to PD-1 inhibitors exhibited lower BDNF expression levels than non-responders (Fig. S3B). In the GSE111414 cohort, due to the limited sample size, the marked variability in BDNF expression within each group resulted in no significant difference being identified between the responder and non-responder groups (Fig. S3C). In the GSE207422 cohort, who received neoadjuvant therapy with

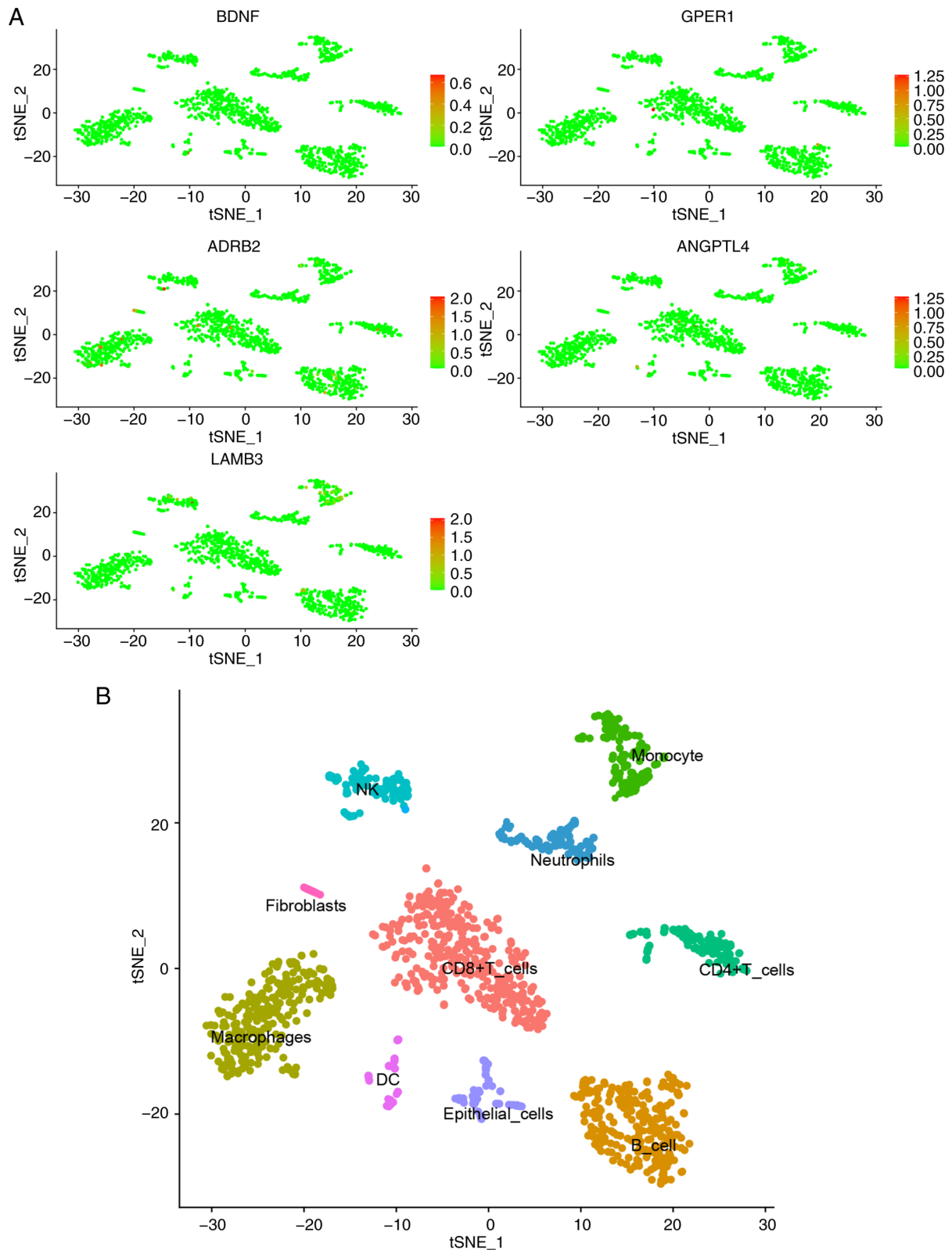


Figure 7. Single-cell analysis. (A) Single-cell gene expression patterns. The expression differences of the six programmed cell death-related genes across various cell populations. Greater red intensity indicates higher expression, while greater green intensity indicates lower expression. (B) Cell type distribution plot. Each colored cluster represents a different cell type. The clear separation between cell types indicates that t-SNE effectively distinguishes between different cell populations. tSNE, t-distributed stochastic neighbor embedding; BDNF, brain-derived neurotrophic factor; GPER1, G protein-coupled estrogen receptor 1; ADRB2, adrenergic receptor b2; ANGPTL4, angiotensin-like protein 4; LAMB3, laminin b3; NK, natural killer; DC, dendritic cell.

PD-1 inhibitors combined with chemotherapy, patients with stage III lung cancer who received this treatment and exhibited a pathological partial response had lower BDNF expression

than that of non-responders (Fig. S3D). These results indicate that the expression levels of BDNF can predict the response of patients with NSCLC to immune checkpoint inhibitor therapy.

Comparison of somatic mutation signatures and TMB. Basic nucleotide variation data were retrieved from TCGA to investigate the differences in genomic mutations between the two risk groups. *TTN* (56%), *TP53* (55%), *CSMD3* (47%), *MUC16* (41%) and *RYR2* (40%) were the top five genes showing the highest mutation frequencies in the high-risk patients (Fig. 8A), and *TP53* (39%), *TTN* (33%), *MUC16* (35%), *CSMD3* (29%) and *RYR2* (32%) were the top five genes in the low-risk group (Fig. 8B). A higher mutation rate was detected in the high-risk group compared with that in the low-risk group ($P < 0.05$). Analysis of somatic mutation interplay revealed widespread gene mutation co-occurrence across the majority of genes. However, *KRAS* and *KEAP1* mutations were mutually exclusive in the high-risk group ($P < 0.05$) (Fig. 8C), while *EGFR* mutations were mutually exclusive (do not co-occur with other genetic mutations within the same chromosomal region) in the low-risk group ($P < 0.05$) (Fig. 8D). Additionally, the high-risk group had a higher TMB ($P < 0.001$) (Fig. 8E). Among patients with LUAD, those in the high-TMB group had a higher OS time compared with those in the low-TMB group ($P = 0.009$) (Fig. 8F). The 2- and 7-year survival rates were significantly lower for patients who were high-risk and had a low-TMB than for patients with other risk and TMB combinations ($P < 0.001$) (Fig. 8G). These outcomes suggested that the current PRG-based model effectively optimizes TMB-based survival predictions. Finally, the mutation rates for the signature PRGs were observed to be as follows: *BDNF* (1.2%), *GPER1* (5%), *ADRB2* (1.4%), *MAP6* (4%), *ANGPTL4* (0.6%) and *LAMB3* (7%) (Fig. 8H).

Exploring potential therapy for patients with LUAD based on the six signature PRGs. Sensitivity analysis of commonly used therapeutic drugs in clinical practice showed that bortezomib, BIBW2992, bleomycin, dasatinib, and bryostatin 1 were more efficacious in the low-risk groups, while camptothecin, CCT007093, ABT.888 and axitinib were more effective in the high-risk group (Fig. 9A). Next, the differentially expressed genes between the two risk groups were categorized into upregulated and downregulated subsets (Fig. 9B). These genes were then queried in the CMap database to identify compounds with potential for the treatment of LUAD. Applying an FDR < 0.05 and standardized score for screening, 10 small-molecule compounds with potential therapeutic effects on LUAD were identified, where a negative enrichment score indicates an antitumor effect (Table I). The three-dimensional structures of the top five small-molecule drugs are displayed in the Fig. 9C. One of the top 10 ranked compounds, namely honokiol, was selected for cytotoxicity validation. An SRB assay (Fig. S4) revealed that at 24 and 48 h, honokiol inhibited the growth of A549 cells in a concentration-dependent manner within the concentration range of 2.5–80 μM , with an IC_{50} of 50 μM . When used in combination with Taxol, honokiol was observed to potentiate the effects of Taxol, allowing for a marked reduction in the required effective dose while maintaining the same therapeutic efficacy. The results of a JC-1 assay indicate that honokiol (50 μM) disrupted the mitochondrial membrane of A549 cells, promoting early apoptosis. When combined with Taxol, this effect was significantly enhanced (Fig. S5). In summary, the PCD prognostic model was used to identify drugs with the potential to effectively treat lung cancer and a

preliminary validation was conducted using cell experiments, which may serve as a reference for the development of novel lung cancer therapies.

Immunohistochemistry validation based on the HPA database. The expression of certain proteins corresponding to the signature PRGs, namely *LAMB3* and *MAP6*, was higher in normal lung tissue than in LUAD tissue (Fig. 10A). However, *ANGPTL4* and *GPER1* did not show clear differences between these tissue types. The expression of *BDNF* in LUAD tissue was higher than that in normal lung tissue. This analysis combined with the current predictive model indicates that the high expression of *BDNF* is negatively associated with the prognosis of patients with LUAD. Notably, it was not possible to evaluate *ADRB2*, as no immunohistochemistry data for this protein is available in the HPA database.

***BDNF* is causally associated with the risk of LUAD.** MR is a reliable method for inferring potential causal relationships, which uses SNPs as IVs to assess causal links between exposure factors and outcomes. MR leverages genetic variations strongly associated with exposure factors as IVs to infer causal effects. All SNPs used in the present study were robust IVs. The causal effects of each genetic variation on LUAD are illustrated in Fig. 10B and C.

A specific analysis of the causal association between *BDNF* levels and LUAD was performed. Using the IVW method, it was demonstrated that higher *BDNF* levels were associated with an increased risk of LUAD, with an odds ratio (OR) of 1.048 (95% CI, 1.002–1.096; $P = 0.04$). However, the MR-Egger method, did not show statistical significance (OR, 1.0717; 95% CI, 1–1.1484; $P = 0.06$). As depicted in Fig. 10D, a systematic MR analysis was conducted by iteratively removing each SNP, and the results remained consistent. This suggests that the causal inference was robust across all SNPs, indicating that no single SNP dominated the association between *BDNF* expression levels and LUAD, thereby validating the MR results. The funnel plot (Fig. 10E) shows a roughly symmetrical distribution, and the MR-Egger regression intercept did not reveal significant horizontal pleiotropy ($P = 0.416$), further supporting the suggestion that that pleiotropy did not bias the causal effect.

Validation of expression of the six signature mRNAs in lung cancer cell lines using RT-qPCR. The expression levels of *BDNF* in LLC ($P < 0.0001$), H1975 ($P < 0.0001$) and A549 ($P < 0.0001$) cells were significantly higher than those in BEAS-2B cells (Fig. 11A). In addition, *GPER1* was also more highly expressed in LLC ($P < 0.001$), H1975 ($P < 0.0001$) and A549 ($P < 0.0001$) cells. However, *ADRB2* as a protective gene, was more highly expressed in BEAS-2B cells than in the three lung cancer cell lines ($P < 0.0001$, respectively). *ANGPTL4* gene expression was higher in H1975 ($P < 0.0001$) and A549 ($P < 0.01$) cells than in BEAS-2B cells, and *LAMB3* expression was elevated in H1975 ($P < 0.0001$) cells compared with BEAS-2B cells. The expression levels of *MAP6* were lower in H1975 cells compared with those in BEAS-2B ($P < 0.0001$) and A549 ($P < 0.05$) cells. These outcomes validate the differential expression of the six PRGs between normal and LUAD samples, highlighting their ability as predictive biomarkers.

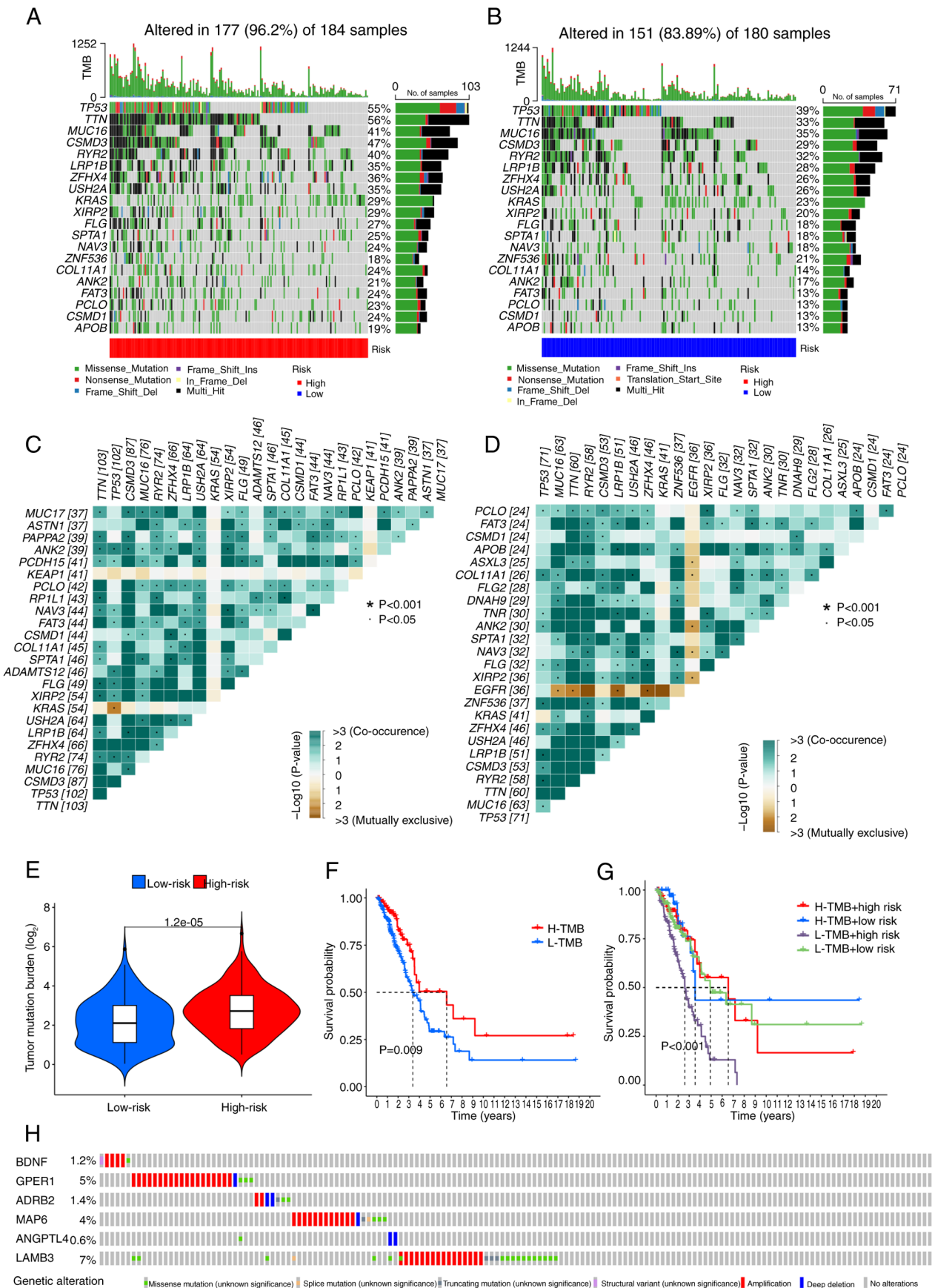


Figure 8. Comparison of somatic mutations and TMB in the six PRGs. Waterfall plots of somatic mutations within the (A) high-risk and (B) low-risk groups. Heatmaps showing the co-occurrence and mutual exclusivity of differentially mutated genes in the (C) high-risk and (D) low-risk categories. The colored blocks represent interactions between mutated genes. A darker cyan color indicates higher co-occurrence, while a darker brown color indicates higher mutual exclusivity. (E) Comparison of TMB levels between the low- and high-risk groups. (F) Survival according to TMB level, categorized into high and low groups. (G) Overall survival disparities according to different combinations of TMB and risk scores. (H) Mutation frequencies of the six PRGs in patients with lung adenocarcinoma sourced from the cBioPortal database. TMB, tumor mutation burden; PRGs, programmed cell death-related genes; H, high; L, low.

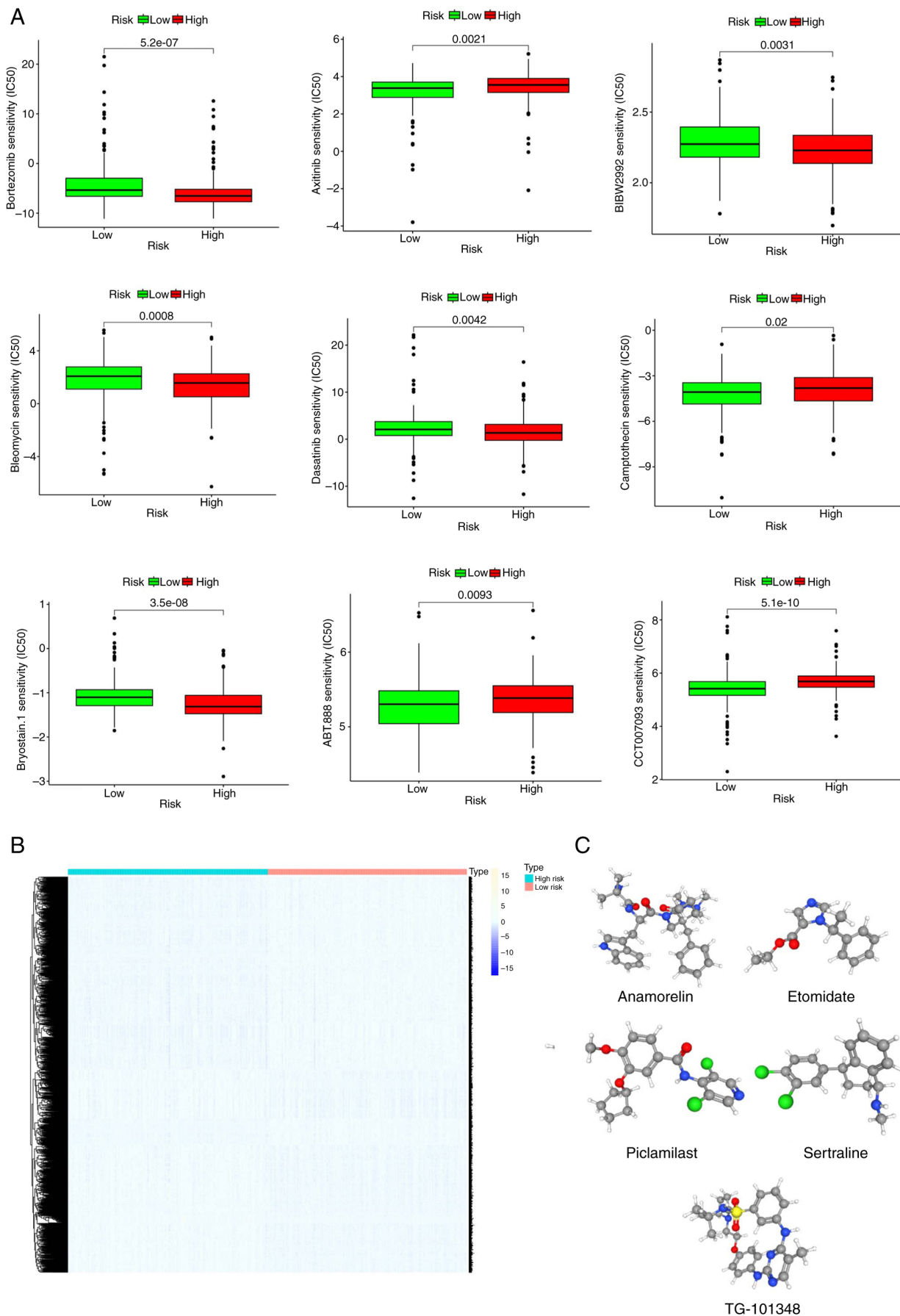


Table I. Small-molecule drugs in the Connectivity Map dataset.

Compound name	Mechanism of action	FDR value	Standardized enrichment score
TG-101348	JAK inhibitor and FLT3 inhibitor	0.0286	-0.6089
Anamorelin	Growth hormone secretagogue receptor agonist	0.0256	-0.6021
Sertraline	Serotonin receptor antagonist	0.0239	-0.6001
Etomidate	Membrane integrity inhibitor	0.0238	-0.6
Piclamilast	Phosphodiesterase inhibitor	0.0185	-0.588
Honokiol	Hippo signaling pathway inhibitor and autophagy agonist	0.0128	-0.572
Spironolactone	Mineralocorticoid receptor antagonist	0.0128	-0.572
BMS-777607	MET inhibitor	0.0078	-0.5542
RS-56812	Serotonin receptor agonist	0.0062	-0.5468
Artesunate	Apoptosis agonist	0.0060	-0.5532

FDR, false discovery rate.

Decreased BDNF expression suppress the growth and migration of lung cancer cells. Based on the results from PPI, LASSO regression and MR, BDNF was identified as the core gene in the six-gene model, as it exhibits a strong positive association with the occurrence and development of LUAD. Therefore, targeted knockdown of BDNF in LLC cells was performed to investigate its importance (Fig. 11B). A colony formation assay (Fig. 11C) revealed that the knockdown of BDNF suppressed the colony formation of LLC cells. Also, the wound healing time of transfected LLC cells was significantly slower compared with that of the si-NC group at 48 h after BDNF knockdown, indicating that BDNF is crucial for the migration of LLC cells (Fig. 11D).

Decreased BDNF expression promotes the PCD of lung cancer cells. Western blot analysis indicated that BDNF knockdown induces apoptosis in LLC cells, as evidenced by caspase-8 cleavage. Whether BDNF knockdown also induces necroptosis was also investigated by the measurement of phosphorylated receptor-interacting protein kinase 1 (p-RIPK1), a phosphorylated protein marker that regulates both apoptosis and necroptosis (36). Notably, LLC cells with BDNF-knockdown exhibited an increased p-RIPK1/RIPK1 ratio ($P < 0.0001$). Similarly, BDNF-knockdown promoted the production of cleaved CASP1 ($P < 0.01$) and cleaved CASP8 ($P < 0.0001$), which are hallmarks of pyroptosis (37) and apoptosis (38) (Fig. S6). In summary, these data suggest that BDNF knockdown sensitizes LLC cells to multiple forms of PCD, including apoptosis, necroptosis and pyroptosis.

Discussion

PCD is an important mechanism for the maintenance of normal cell renewal and tissue homeostasis via the removal of potentially harmful, dysfunctional or damaged cells. Dysregulation of the normal cell death process can lead to various human diseases, including autoimmune diseases, cancer, infectious diseases, neurodegenerative diseases and cardiovascular diseases (39). Apoptosis is a well-established example of PCD, which is involved in embryonic development, the removal of

infected cells and clearance of abnormal cells (40). Apoptosis is a key mechanism targeted by numerous cancer therapies. However, cancer cells can develop chemoresistance by evading apoptosis. For example, the upregulation of miRNA-34a and miR-141 during treatment may contribute to the paclitaxel resistance of breast cancer cell lines (41). Another mode of PCD is pyroptosis, a novel non-apoptotic form of PCD closely associated with inflammatory responses. Pyroptosis is mainly triggered by inflammasomes and executed by the caspase and gasdermin protein families. Pyroptosis kills tumor cells by releasing cytokines, including IL-18 and IL-1 β , and other molecules, such as high mobility group box 1 protein and ATP, and activating antitumor immunity (42). PCD has been indicated to play a crucial role in cancer clinical therapy and the development of diagnostic markers. Although molecular prognostic models for LUAD have been developed, their effectiveness remains limited. Also, numerous models focusing on cell death consider only a single type of cell death, neglecting the interactions and crosstalk between different cell death pathways (43-46).

In the present study, the key genes of 15 different PCD modules were extensively screened and six PRGs associated with the prognosis of LUAD were identified: BDNF, GPER1, ADRB2, MAP6, ANGPTL4 and LAMB3. The differential expression of these PRGs in LUAD cell lines was demonstrated using RT-qPCR. In addition, KEGG and GO enrichment analyses were performed to investigate the biological roles of PRGs in LUAD. A prognostic model was developed using TCGA cohort as the training set, while GEO cohorts served as validation sets to assess the reliability of the model. The PRG model was used to calculate a risk score for patients with LUAD, and this score was shown to independently predict patient prognosis. In addition, a prognostic nomogram encompassing clinical features and risk scores was constructed, and the associations between risk scores and the TME were analyzed. Finally, the causal relationship between the core gene BDNF and LUAD was explored through MR, and preliminary validation was performed via cell experiments.

The present study discovered that the expression levels of ADRB2 and MAP6 are elevated in patients with

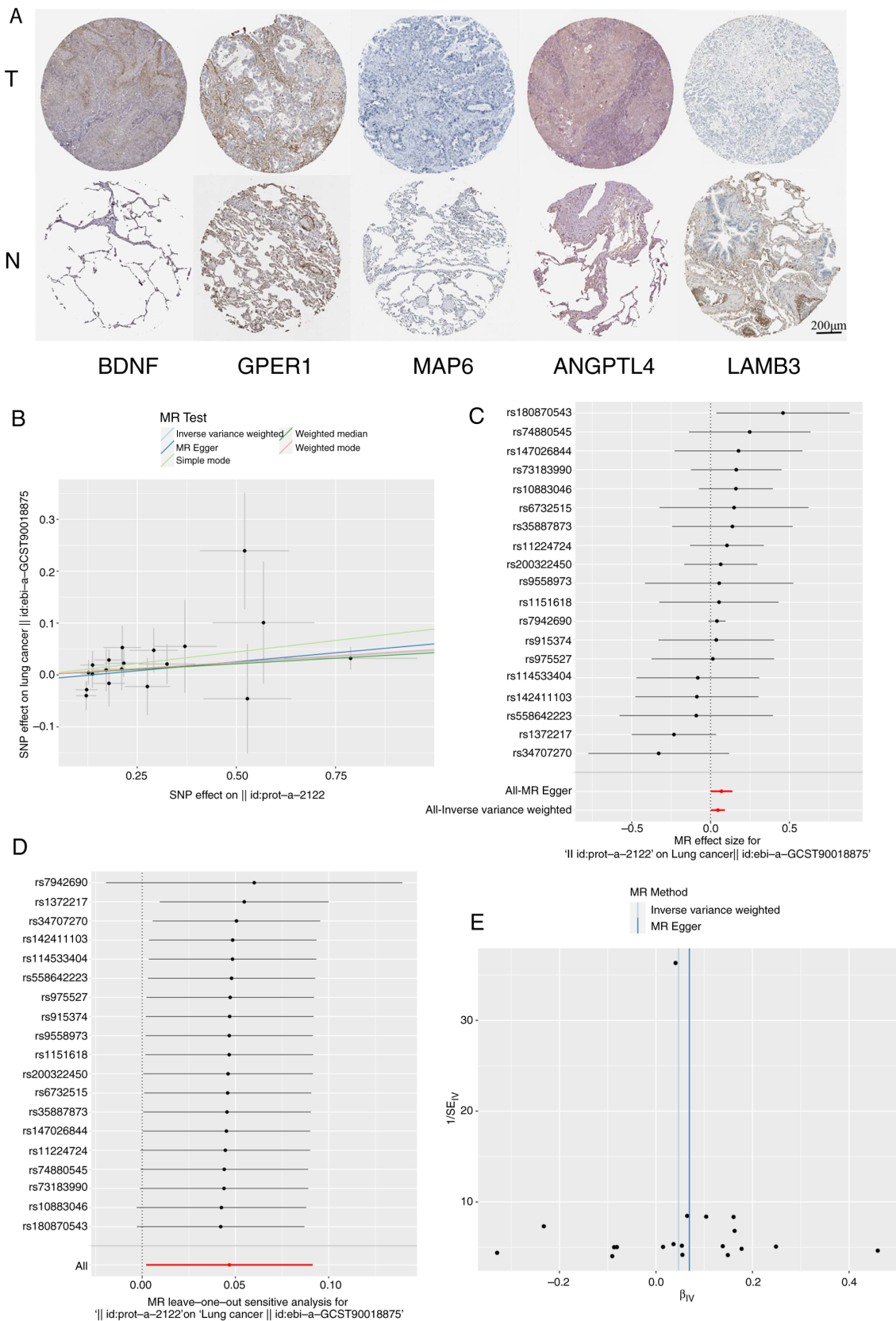


Figure 10. Protein expression of five PRGs and MR analysis results. (A) Immunohistochemistry results from the Human Protein Atlas database (proteinatlas.org) showing the protein expression of five signature PRGs (BDNF: <https://www.proteinatlas.org/ENSG00000176697-BDNF/tissue>; GPER1: <https://www.proteinatlas.org/ENSG00000164850-GPER1/tissue>; MAP6: <https://www.proteinatlas.org/ENSG00000171533-MAP6/tissue>; ANGPTL4: <https://www.proteinatlas.org/ENSG00000196878-ANGPTL4/tissue>; LAMB3: <https://www.proteinatlas.org/ENSG00000196878-LAMB3/tissue>). (B) Scatter plot illustrating the causal effect of BDNF on LUAD risk. (C) Forest plot depicting the causal effect of each SNP on the risk of LUAD. (D) Leave-one-out plot visualizing the causal effect of BDNF on LUAD risk with each SNP excluded one at a time. (E) Funnel plots to assess the overall heterogeneity of MR estimates for the effect of BDNF on LUAD. PRGs, programmed cell death-related genes; MR, Mendelian randomization; BDNF, brain-derived neurotrophic factor; LUAD, lung adenocarcinoma; SNP, single nucleotide polymorphism; GPER1, G protein-coupled estrogen receptor 1; MAP6, microtubule associated protein 6; ANGPTL4, angiopoietin-like protein 4; LAMB3, laminin b3.

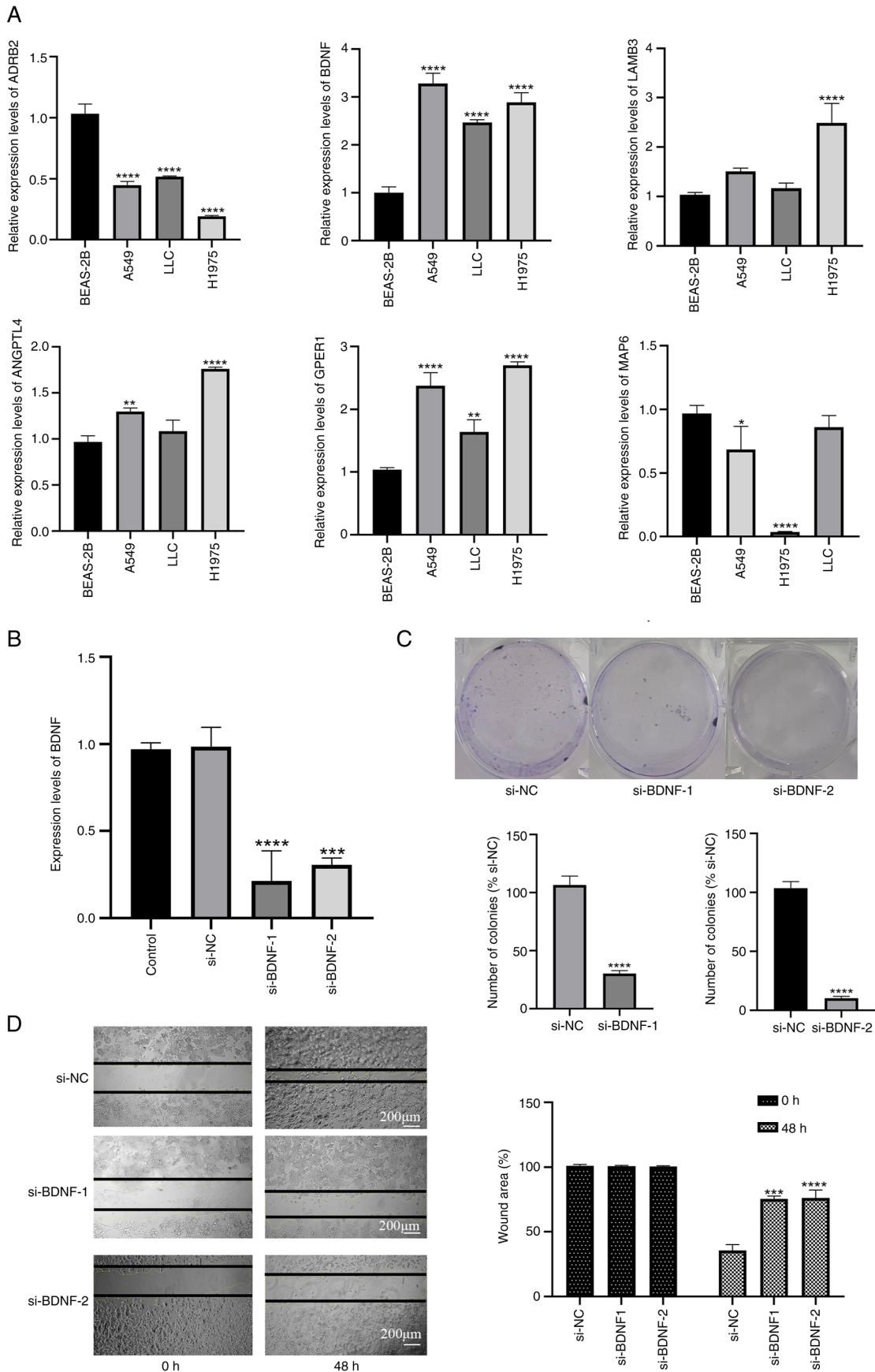


Figure 11. Knockdown of BDNF effectively inhibits the growth and migration of lung cancer cells. (A) mRNA expression of six predictive PRGs in lung cancer and normal human bronchial epithelial cell lines. (B) BDNF gene expression in A549 cells is effectively reduced by si-BDNF. (C) Cell growth evaluated by colony formation assay (n=3). (D) Cell migration evaluated by wound healing assay using three randomized microscopic fields (n=3). Data are presented as the mean \pm SD. * $P < 0.05$, ** $P < 0.01$, *** $P < 0.001$ and **** $P < 0.0001$ vs. BEAS-2B, control or si-NC, as appropriate. LLC, Lewis lung carcinoma; BDNF, brain-derived neurotrophic factor; ADRB2, adrenergic receptor b2; ANGPTL4, angiopoietin-like protein 4; GPER1, G protein-coupled estrogen receptor 1; LAMB3, laminin b3; MAP6, microtubule associated protein 6; si, small interfering RNA; NC, negative control.

LUAD and associated with an improved prognosis, while the elevated expression of *BDNF*, *GPER1*, *ANGPTL4* and *LAMB3* is associated with a poor prognosis. Based on the PPI network, LASSO regression and coefficient scoring, *BDNF* was identified as the core gene with the highest efficacy in the model. The causal relationship between *BDNF* and LUAD was determined via MR analysis, indicating that the elevated expression of *BDNF* is an important factor in the occurrence and development of LUAD. *In vitro* experiments demonstrated that reducing the level of *BDNF* effectively restrained the invasion and proliferation of lung cancer cells. *BDNF* is a member of the NT family and plays a crucial role in neuronal development and regeneration (19). Upon binding with its main receptor TrkB, *BDNF* activates diverse downstream signaling pathways, including the RAS, PI3K/AKT and JAK/STAT pathways (47). *BDNF* is mainly secreted by tumor cells and promotes tumor growth and survival in patients with cancer, with research demonstrating that *BDNF* and TrkB facilitate the onset and progression of various human malignancies, including lung (48), breast (49), prostate (50) and colorectal (51) cancer. *BDNF*/TrkB signaling has been reported to be associated with proliferation and invasiveness, suggesting that *BDNF* may be a crucial element in tumor progression and a potential therapeutic target (52).

In addition to the ability of the six-gene risk score to assess the prognosis of patients with LUAD, it is noteworthy that the low-risk score group exhibited higher levels of DC, CD8⁺ T cell, Th1 cell, NK cell and B cell infiltration than the high-risk score group. DCs, Th1 cells and CD8⁺ T cells are key participants in antitumor-specific immunity, while B cells represent humoral antitumor immunity and activate NK cells through antibody-dependent cellular cytotoxicity (53). The results of the present study suggest that patients in the low-risk group have a stronger antitumor adaptive immune response, potentially forming an immune memory that improves prognosis. However, the low-risk group also had an increased TIDE score, indicating increased immune evasion, which suggests a hidden risk of immune cell exhaustion. The expression of immune checkpoint markers was higher in the low-risk group compared with the high-risk group, indicating that the use of immune checkpoint inhibitors might yield promising results for low-risk patients. In the high-risk group, the TME accumulated high levels of factors such as CAFs, which can result in CD8⁺ T cell exhaustion and subsequent tumor immune evasion (54). Additionally, based on the somatic mutation waterfall plot, *TP53* missense mutations were found to be among the most frequent mutations in both groups, with the mutation rates of *TP53* and *KRAS* being higher in the high-risk group compared with those in the low-risk group. *TP53* is a crucial tumor suppressor gene, and its high frequency of missense mutations often indicates a poor prognosis for patients (55). A strong mutual exclusivity between *KRAS* and *TP53* was observed in the high-risk group, while in the low-risk group, *EGFR* showed strong mutual exclusivity with *MUC16*, *TTN*, *LRP1B* and *ZFH4*. A cohort study of 283 lung cancer cytology samples indicated that patients with the *KRAS/TP53* subtype had worse OS compared with patients with other subtypes (56). Based on the prognostic model and somatic mutation results

obtained in the present study, a TMB analysis was conducted between the high- and low-risk groups to guide immunotherapy and survival prediction. The results demonstrated that the 2- and 7-year survival rates were significantly lower in patients with high-risk and a low-TMB group compared with that in patients with other risk and TMB combinations, suggesting that the PRG model effectively optimizes TMB-based survival predictions. To validate the predictive role of *BDNF* in immunotherapy, four GEO immunotherapy cohorts were evaluated. The results of this evaluation indicate that *BDNF* expression levels may help to determine whether PD-1/PD-L1 inhibitors are likely to be beneficial in the systemic or neoadjuvant treatment of patients with advanced-stage NSCLC.

A number of researchers have found a close relationship between PCD activity and antitumor immune responses, consistent with the results of the present study. PCD can be classified into immunogenic and non-immunogenic types, depending on its ability to initiate adaptive immune responses. Immunogenic PCD alerts the immune system to potential threats by releasing pro-inflammatory cytokines or damage-associated molecular patterns. Pattern recognition receptors on immune cells detect these signals, which then trigger the activation of immune responses (57). For instance, necroptotic cells promote DC maturation and cross-priming efficiency, thereby boosting CD8⁺ T cell-mediated antitumor immunity through RIPK1 and NF- κ B signaling pathways (58).

Notably, the risk score also performed well in guiding chemotherapy strategies. The present study found that patients in the high-risk group had higher IC₅₀ values for axitinib, veliparib (ABT-888) and camptothecin, which could explain the poorer prognosis of patients due to their resistance to these drugs. Conversely, the high-risk group exhibited lower IC₅₀ values for bortezomib, bleomycin and bryostatins 1, suggesting that these drugs could be potential candidates for treating patients with LUAD who have become resistant to standard treatments. Furthermore, differentially expressed genes were screened between high- and low-risk groups, and imported into the CMap database, which identified 10 compounds with potential therapeutic efficacy for patients with high-risk LUAD. These compounds included fedratinib (TG-101348), a JAK2 inhibitor that has demonstrated therapeutic efficacy in patients with primary or secondary myelofibrosis (59). Studies have shown that the combination of fedratinib and erlotinib can inhibit the growth of erlotinib-resistant NSCLC cells by suppressing the JAK2/STAT3 signaling pathway (60). Another compound identified was anamorelin, a novel non-peptide ghrelin receptor agonist primarily used to treat cachexia, which addresses factors such as appetite, body composition, adipose tissue metabolism, energy expenditure and inflammation. Two international, double-blind, phase III trials, known as ROMANA 1 and ROMANA 2, have established the efficacy and safety of anamorelin in patients with advanced NSCLC and cachexia (61). Further identified compounds included sertraline, an antidepressant with anticancer properties that enhances TRAIL-mediated apoptosis in lung cancer cells mainly via the downregulation of AMP-activated protein kinase phosphorylation (62), and etomidate, a non-barbiturate intravenous anesthetic that

modulates g-aminobutyric acid type A receptors to induce anesthesia, and has been shown to sustain CD4⁺ and CD8⁺ T cell levels in patients with LUAD (63). Furthermore, cellular experiments have shown that etomidate inhibits the migration and invasion of A549 cells by suppressing the expression of MMP1, MMP2, MMP7 and MMP9 (64). The present study suggests that these drugs also have the potential to regulate PCD in LUAD, which warrants further mechanistic investigations.

Although the present study offers worthwhile insights into the clinical significance of PCD characteristics and BDNF, several limitations must be acknowledged. First, certain analyses are based on retrospective data from public databases, which emphasizes the requirement for prospective studies to confirm the clinical importance of the findings. Considering the complexity and diverse histological phenotypes of LUAD, more detailed mechanistic and clinical research is essential to investigate the roles of PRGs across different LUAD subtypes. Also, although the differential expression of PRGs between LUAD and precancerous specimens has been analyzed, protein-level validation of these genes remains pending. In addition, comprehensive *in vivo* and *in vitro* experiments are warranted to further elucidate the mechanistic roles of BDNF in tumor progression and its interaction with the TME. Lastly, the impact of the PCD model in the present study has yet to be confirmed through phase III randomized controlled trials. Therefore, it is proposed that future research should involve superior, adequately followed up, large-sample, multicenter randomized controlled trials to substantiate the findings of the present study.

In summary, the present study discerned molecular subtypes of LUAD via the detection of PRGs and established a prognostic signature. Additionally, immune infiltration landscapes, gene mutation status and drug predictions for different risk groups were analyzed. The prognostic signature may be used to enhance the clinical evaluation of patient prognosis and guide drug therapy decisions.

Acknowledgements

Not applicable.

Funding

No funding was received.

Availability of data and materials

The data generated in the present study may be requested from the corresponding author.

Authors' contributions

JX, CZ and BS conceived and designed the study. JX, WZ, LD, SY, ST, LY, CF, XZ and ZH collected and analyzed the data. JX, WZ, LD, SY and ST wrote the manuscript. CZ and BS contributed materials. JX, CZ and BS confirm the authenticity of all the raw data. All authors read and approved the final version of the manuscript.

Ethics approval and consent to participate

Not applicable.

Patient consent for publication

Not applicable.

Competing interests

The authors declare that they have no competing interests.

References

- Sung H, Ferlay J, Siegel RL, Laversanne M, Soerjomataram I, Jemal A and Bray F: Global cancer statistics 2020: GLOBOCAN Estimates of incidence and mortality worldwide for 36 cancers in 185 countries. *CA Cancer J Clin* 71: 209-249, 2021.
- Testa U, Castelli G and Pelosi E: Lung cancers: Molecular characterization, clonal heterogeneity and evolution, and cancer stem cells. *Cancers (Basel)* 10: 248, 2018.
- Song J, Sun Y, Cao H, Xi L, Dong C, Yang R and Shi Y: A novel pyroptosis-related lncRNA signature for prognostic prediction in patients with lung adenocarcinoma. *Bioengineered* 12: 5932-5949, 2021.
- Al-Dherasi A, Huang QT, Liao Y, Al-Mosaib S, Hua R, Wang Y, Yu Y, Zhang Y, Zhang X, Huang C, *et al.*: A seven-gene prognostic signature predicts overall survival of patients with lung adenocarcinoma (LUAD). *Cancer Cell Int* 21: 294, 2021.
- Miller KD, Siegel RL, Lin CC, Mariotto AB, Kramer JL, Rowland JH, Stein KD, Alteri R and Jemal A: Cancer treatment and survivorship statistics, 2016. *CA Cancer J Clin* 66: 271-289, 2016.
- Liu J, Hong M, Li Y, Chen D, Wu Y and Hu Y: Programmed cell death tunes tumor immunity. *Front Immunol* 13: 847345, 2022.
- Wang S, Wang R, Hu D, Zhang C, Cao P and Huang J: Machine learning reveals diverse cell death patterns in lung adenocarcinoma prognosis and therapy. *NPJ Precis Oncol* 8: 49, 2024.
- Liu T, Zhu C, Chen X, Guan G, Zou C, Shen S, Wu J, Wang Y, Lin Z, Chen L, *et al.*: Ferroptosis, as the most enriched programmed cell death process in glioma, induces immunosuppression and immunotherapy resistance. *Neuro Oncol* 24: 1113-1125, 2022.
- Singh P and Lim B: Targeting apoptosis in cancer. *Curr Oncol Rep* 24: 273-284, 2022.
- Qin Y, Ashrafizadeh M, Mongiardini V, Grimaldi B, Crea F, Rietdorf K, Gyórfy B, Kliionsky DJ, Ren J, Zhang W and Zhang X: Autophagy and cancer drug resistance in dialogue: Pre-clinical and clinical evidence. *Cancer Lett* 570: 216307, 2023.
- Tong X, Tang R, Xiao M, Xu J, Wang W, Zhang B, Liu J, Yu X and Shi S: Targeting cell death pathways for cancer therapy: Recent developments in necroptosis, pyroptosis, ferroptosis, and cuproptosis research. *J Hematol Oncol* 15: 174, 2022.
- Ma X, Xiao L, Liu L, Ye L, Su P, Bi E, Wang Q, Yang M, Qian J and Yi Q: CD36-mediated ferroptosis dampens intratumoral CD8(+) T cell effector function and impairs their antitumor ability. *Cell Metab* 33: 1001-1012.e1005, 2021.
- Zhang C, Xia J, Liu X, Li Z, Gao T, Zhou T and Hu K: Identifying prognostic genes related PANoptosis in lung adenocarcinoma and developing prediction model based on bioinformatics analysis. *Sci Rep* 13: 17956, 2023.
- Xu K, Zhang Y, Yan Z, Wang Y, Li Y, Qiu Q, Du Y, Chen Z and Liu X: Identification of disulfidptosis related subtypes, characterization of tumor microenvironment infiltration, and development of DRG prognostic prediction model in RCC, in which *MSH3* is a key gene during disulfidptosis. *Front Immunol* 14: 1205250, 2023.
- Tian Q, Zhou Y, Zhu L, Gao H and Yang J: Development and validation of a ferroptosis-related gene signature for overall survival prediction in lung adenocarcinoma. *Front Cell Dev Biol* 9: 684259, 2021.
- Liang JY, Wang DS, Lin HC, Chen XX, Yang H, Zheng Y and Li YH: A novel ferroptosis-related gene signature for overall survival prediction in patients with hepatocellular carcinoma. *Int J Biol Sci* 16: 2430-2441, 2020.

17. Wei J, Zeng Y, Gao X and Liu T: A novel ferroptosis-related lncRNA signature for prognosis prediction in gastric cancer. *BMC Cancer* 21: 1221, 2021.
18. Ricci A, Salvucci C, Castelli S, Carraturo A, de Vitis C and D'Ascanio M: Adenocarcinomas of the lung and neurotrophin system: A review. *Biomedicines* 10: 2531, 2022.
19. Zhang SY, Hui LP, Li CY, Gao J, Cui ZS and Qiu XS: More expression of BDNF associates with lung squamous cell carcinoma and is critical to the proliferation and invasion of lung cancer cells. *BMC Cancer* 16: 171, 2016.
20. Zhang ZX, Yong Y, Tan WC, Shen L, Ng HS and Fong KY: Prognostic factors for mortality due to pneumonia among adults from different age groups in Singapore and mortality predictions based on PSI and CURB-65. *Singapore Med J* 59: 190-198, 2018.
21. Sinkevicius KW, Kriegel C, Bellaria KJ, Lee J, Lau AN, Leeman KT, Zhou P, Beede AM, Fillmore CM, Caswell D, *et al*: Neurotrophin receptor TrkB promotes lung adenocarcinoma metastasis. *Proc Natl Acad Sci USA* 111: 10299-10304, 2014.
22. Yu Q, Wang Y, Yi G, Yang W, Chen K, Tan X, Zhang X, Xu Z, Yang Z and Peng Y: BDNF is a prognostic biomarker involved in immune infiltration of lung adenocarcinoma and is associated with brain metastasis. *Immunology* 168: 320-330, 2023.
23. Bergman PJ: Cancer immunotherapy. *Vet Clin North Am Small Anim Pract* 54: 441-468, 2024.
24. Lee ES, Son DS, Kim SH, Lee J, Jo J, Han J, Kim H, Lee HJ, Choi HY, Jung Y, *et al*: Prediction of recurrence-free survival in postoperative non-small cell lung cancer patients by using an integrated model of clinical information and gene expression. *Clin Cancer Res* 14: 7397-7404, 2008.
25. Zhou X, Xiao B, Jiang M and Rui J: **Pan-cancer analysis identifies EMC6 as a potential target for lung adenocarcinoma.** *iScience* 27: 108648, 2023.
26. Rousseaux S, Debernardi A, Jacquiau B, Vitte AL, Vesin A, Nagy-Mignotte H, Moro-Sibilot D, Brichon PY, Lantuejoul S, Hainaut P, *et al*: Ectopic activation of germline and placental genes identifies aggressive metastasis-prone lung cancers. *Sci Transl Med* 5:186ra66, 2013.
27. Hight SK, Mootz A, Kollipara RK, McMillan E, Yenerall P, Otaki Y, Li LS, Avila K, Peyton M, Rodriguez-Canales J, *et al*: An in vivo functional genomics screen of nuclear receptors and their co-regulators identifies FOXA1 as an essential gene in lung tumorigenesis. *Neoplasia* 22: 294-310, 2020.
28. Langfelder P and Horvath S: WGCNA: An R package for weighted correlation network analysis. *BMC Bioinformatics* 9: 559, 2008.
29. Hu J, Zhang L, Xia H, Yan Y, Zhu X, Sun F, Sun L, Li S, Li D, Wang J, *et al*: Tumor microenvironment remodeling after neoadjuvant immunotherapy in non-small cell lung cancer revealed by single-cell RNA sequencing. *Genome Med* 15: 14, 2023.
30. Trefny MP, Rothschild SI, Uhlenbrock F, Rieder D, Kasenda B, Stanczak MA, Berner F, Kashyap AS, Kaiser M, Herzig P, *et al*: A variant of a killer cell immunoglobulin-like receptor is associated with resistance to PD-1 blockade in lung cancer. *Clin Cancer Res* 25: 3026-3034, 2019.
31. Cho JW, Hong MH, Ha SJ, Kim YJ, Cho BC, Lee I and Kim HR: Genome-wide identification of differentially methylated promoters and enhancers associated with response to anti-PD-1 therapy in non-small cell lung cancer. *Exp Mol Med* 52: 1550-1563, 2020.
32. Kim JY, Choi JK and Jung H: Genome-wide methylation patterns predict clinical benefit of immunotherapy in lung cancer. *Clin Epigenetics* 12: 119, 2020.
33. Malta TM, Sokolov A, Gentles AJ, Burzykowski T, Poisson L, Weinstein JN, Kamińska B, Huelsken J, Omberg L, Gevaert O, *et al*: Machine learning identifies stemness features associated with oncogenic dedifferentiation. *Cell* 173: 338-354, e15, 2018.
34. Gao Y, Kim S, Lee YI and Lee J: Cellular stress-modulating drugs can potentially be identified by in silico screening with connectivity map (CMap). *Int J Mol Sci* 20: 5601, 2019.
35. Livak KJ and Schmittgen TD: **Analysis of relative gene expression data using real-time quantitative PCR and the 2(-Delta Delta C(T)) method.** *Methods* 25: 402-408, 2001.
36. Mifflin L, Ofengime D and Yuan J: Receptor-interacting protein kinase 1 (RIPK1) as a therapeutic target. *Nat Rev Drug Discov* 19: 553-571, 2020.
37. Wang X, Chen Z, Nie D, Zeng X, Zhong M, Liu X, Zhong S, Wang L, Liao Z, Chen C, *et al*: CASP1 is a target for combination therapy in pancreatic cancer. *Eur J Pharmacol* 961: 176175, 2023.
38. Hattori T, Fundora KA, Hamamoto K, Opozda DM, Liang X, Liu X, Zhang J, Uzun Y, Takahashi Y and Wang HG: ER stress elicits non-canonical CASP8 (caspase 8) activation on autophagosomal membranes to induce apoptosis. *Autophagy* 20: 349-364, 2024.
39. Hu J, Pan D, Li G, Chen K and Hu X: Regulation of programmed cell death by Brd4. *Cell Death Dis* 13: 1059, 2022.
40. Hsu SK, Li CY, Lin IL, Syue WJ, Chen YF, Cheng KC, Teng YN, Lin YH, Yen CH and Chiu CC: Inflammation-related pyroptosis, a novel programmed cell death pathway, and its crosstalk with immune therapy in cancer treatment. *Theranostics* 11: 8813-8835, 2021.
41. Hsu SK, Chang WT, Lin IL, Chen YF, Padalwar NB, Cheng KC, Teng YN, Wang CH and Chiu CC: The role of necroptosis in ROS-mediated cancer therapies and its promising applications. *Cancers (Basel)* 12: 2185, 2020.
42. Khan M, Ai M, Du K, Song J, Wang B, Lin J, Ren A, Chen C, Huang Z, Qiu W, *et al*: Pyroptosis relates to tumor microenvironment remodeling and prognosis: A pan-cancer perspective. *Front Immunol* 13: 1062225, 2022.
43. Pan S, Meng H, Fan T, Hao B, Song C, Li D, Li N and Geng Q: Comprehensive analysis of programmed cell death signature in the prognosis, tumor microenvironment and drug sensitivity in lung adenocarcinoma. *Front Genet* 13: 900159, 2022.
44. Yang S, Ji J, Wang M, Nie J and Wang S: Construction of ovarian cancer prognostic model based on the investigation of ferroptosis-related lncRNA. *Biomolecules* 13: 306, 2023.
45. Chen H, Luo H, Wang J, Li J and Jiang Y: Identification of a pyroptosis-related prognostic signature in breast cancer. *BMC Cancer* 22: 429, 2022.
46. Chen Y, Huang W, Ouyang J, Wang J and Xie Z: Identification of anoikis-related subgroups and prognosis model in liver hepatocellular carcinoma. *Int J Mol Sci* 24: 2862, 2023.
47. Malekan M, Nezamabadi SS, Samami E, Mohebalizadeh M, Saghazadeh A and Rezaei N: BDNF and its signaling in cancer. *J Cancer Res Clin Oncol* 149: 2621-2636, 2023.
48. Yeo IJ, Yu JE, Kim SH, Kim DH, Jo M, Son DJ, Yun J, Han SB and Hong JT: TNF receptor 2 knockout mouse had reduced lung cancer growth and schizophrenia-like behavior through a decrease in TrkB-dependent BDNF level. *Arch Pharm Res* 47: 341-359, 2024.
49. Goto T, Saligan LN, Li X, Xiang L, Kwiat C, Nguyen C, Crouch A and Von Ah D: Associations of brain-derived neurotrophic factor rs6265 polymorphism and cognitive function in breast cancer survivors from a cross-sectional study. *Cancer Med* 13: e6975, 2024.
50. Liu YN, Chen WY, Liu MK, Yeh HL, Chen WH, Jiang KC, Li HR, Chen ZQ, Wang WH, Abou-Kheir W and Wen YC: Immunosuppressive role of BDNF in therapy-induced neuroendocrine prostate cancer. *Mol Oncol* 18: 1665-1686, 2024.
51. Večurková I, Mašlanková J, Tomečková V, Kaťuchová J, Kisková T, Fröhlichová L, Mareková M and Stupák M: Stage-dependent levels of brain-derived neurotrophic factor and matrix metalloproteinase 9 in the prognosis of colorectal cancer. *Biomedicines* 11: 1839, 2023.
52. Tian J, Cheng H, Wang N and Wang C: SLERT, as a novel biomarker, orchestrates endometrial cancer metastasis via regulation of BDNF/TRKB signaling. *World J Surg Oncol* 21: 27, 2023.
53. Park JE, Kim SE, Keam B, Park HR, Kim S, Kim M, Heo DS, Doh J, Kim DW and Heo DS: Anti-tumor effects of NK cells and anti-PD-L1 antibody with antibody-dependent cellular cytotoxicity in PD-L1-positive cancer cell lines. *J Immunother Cancer* 8: 2020.
54. Li X, Sun Z, Peng G, Xiao Y, Guo J, Wu B, Li X, Zhou W, Li J, Li J, Ba C, *et al*: Single-cell RNA sequencing reveals a pro-invasive cancer-associated fibroblast subgroup associated with poor clinical outcomes in patients with gastric cancer. *Theranostics* 12: 620-638, 2022.
55. Zhang W, Edwards A, Flemington EK and Zhang K: Significant Prognostic Features and Patterns of Somatic TP53 Mutations in Human Cancers. *Cancer Inform* 16: 1176935117691267, 2017.
56. Ruiz-Cordero R, Ma J, Khanna A, Lyons G, Rinsurongkawong W, Bassett W, Guo M, Routbort MJ, Zhang J, Skoulidis F, *et al*: Simplified molecular classification of lung adenocarcinomas based on EGFR, KRAS, and TP53 mutations. *BMC Cancer* 20: 83, 2020.
57. Green DR, Ferguson T, Zitvogel L and Kroemer G: Immunogenic and tolerogenic cell death. *Nat Rev Immunol* 9: 353-363, 2009.

58. Yatim N, Jusforgues-Saklani H, Orozco S, Schulz O, Barreira da Silva R, Reis e Sousa C, Green DR, Oberst DR and Albert V: RIPK1 and NF- κ B signaling in dying cells determines cross-priming of CD8+ T cells. *Science* 350: 328-334, 2015.
59. Pardanani A, Harrison C, Cortes JE, Cervantes F, Mesa RA, Milligan D, Masszi T, Mishchenko E, Jourdan E, Vannucchi AM, *et al*: Safety and efficacy of fedratinib in patients with primary or secondary myelofibrosis: A randomized clinical trial. *JAMA Oncol* 1: 643-651, 2015.
60. Chen D, Zhang F, Wang J, He H, Duan S, Zhu R, Chen C, Yin L and Chen Y: Biodegradable nanoparticles mediated co-delivery of erlotinib (ELTN) and fedratinib (FDTN) toward the treatment of ELTN-resistant non-small cell lung cancer (NSCLC) via suppression of the JAK2/STAT3 signaling pathway. *Front Pharmacol* 9: 1214, 2018.
61. Currow D, Temel JS, Abernethy A, Milanowski J, Friend J and Fearon KC: ROMANA 3: A phase 3 safety extension study of anamorelin in advanced non-small-cell lung cancer (NSCLC) patients with cachexia. *Ann Oncol* 28: 1949-1956, 2017.
62. Zinnah KMA, Seol JW and Park SY: Inhibition of autophagy flux by sertraline attenuates TRAIL resistance in lung cancer via death receptor 5 upregulation. *Int J Mol Med* 46: 795-805, 2020.
63. Liu J, Dong W, Wang T, Liu L, Zhan L, Shi Y and Han J: Effects of etomidate and propofol on immune function in patients with lung adenocarcinoma. *Am J Transl Res* 8: 5748-5755, 2016.
64. Chu CN, Wu KC, Chung WS, Zheng LC, Juan TK, Hsiao YT, Peng SF, Yang JL, Ma YS, Wu RS and Chung JG: Etomidate suppresses invasion and migration of human A549 lung adenocarcinoma cells. *Anticancer Res* 39: 215-223, 2019.



Copyright © 2025 Xia et al. This work is licensed under a Creative Commons Attribution-NonCommercial-NoDerivatives 4.0 International (CC BY-NC-ND 4.0) License.